ELOVL4: Very long-chain fatty acids serve an eclectic role in mammalian health and function

Blake R. Hopiavuori[a,b,1], **Robert E. Anderson**[a,b,c,d,f,*,1], **Martin-Paul Agbaga**[a,b,c,d,e,**,1]

[a]Oklahoma Center for Neurosciences, University of Oklahoma Health Sciences Center, Oklahoma City, OK 73104, USA

[b]Dean McGee Eye Institute, University of Oklahoma Health Sciences Center, Oklahoma City, OK 73104, USA

[c]Department of Ophthalmology, University of Oklahoma Health Sciences Center, Oklahoma City, OK 73104, USA

[d]Department of Cell Biology, University of Oklahoma Health Sciences Center, Oklahoma City, OK 73104, USA

[e]Harold Hamm Diabetes Center, University of Oklahoma Health Sciences Center, Oklahoma City, OK 73104, USA

[f]Reynolds Oklahoma Center on Aging, Department of Geriatric Medicine, University of Oklahoma Health Sciences Center, Oklahoma City, OK 73104, USA

Abstract

ELOngation of **V**ery **L**ong chain fatty acids-**4** (ELOVL4) is an elongase responsible for the biosynthesis of very long chain (VLC, $\geq$ C28) saturated (VLC-SFA) and polyunsaturated (VLC-PUFA) fatty acids in brain, retina, skin, Meibomian glands, and testes. Fascinatingly, different mutations in this gene have been reported to cause vastly different phenotypes in humans. Heterozygous inheritance of seven different mutations in the coding sequence and 5' untranslated region of *ELOVL4* causes autosomal dominant Stargardt-like macular dystrophy (STGD3), while homozygous inheritance of three more mutant variants causes severe seizures with ichthyosis, hypertonia, and even death. Some recent studies have described heterozygous inheritance in yet another three mutant *ELOVL4* variants, two that cause spinocerebellar ataxia-34 (SCA34) with erythrokeratodermia (EKV) and one that causes SCA34 without EKV. We identified the specific enzymatic reactions catalyzed by ELOVL4 and, using a variety of genetically engineered mouse models, have actively searched for the mechanisms by which ELOVL4 impacts neural function and health. In this review, we critically compare and contrast the various animal model and

*Corresponding author. Dean McGee Eye Institute, University of Oklahoma Health Sciences Center, Oklahoma City, OK 73104, USA. robert-anderson@ouhsc.edu (R.E. Anderson). **Corresponding author. Dean McGee Eye Institute, University of Oklahoma Health Sciences Center, Oklahoma City, OK 73104, USA. martin-paul-agbaga@ouhsc.edu (M.-P. Agbaga).
[1]Percentage of work contributed by each author in the production of the manuscript is as follows: Blake Hopiavuori (34%), Robert Anderson (33%), Martin-Paul Agbaga (33%).

Author Manuscript

case studies involving ELOVL4 deficiency via either mutation or deletion, and the resulting consequences on neuronal health and function in both the retina and central nervous system.

Keywords

Stargardt; ELOVL4; Spinocerebellar ataxia; Very long-chain fatty acids; VLC-PUFA; VLC-SFA

1.   Discovery of multiple mutations in fatty acid elongase-4 (*ELOVL4*) as the cause of Stargardt-like macular dystrophy

Autosomal dominant Stargardt-like macular dystrophy (STGD3) results in early onset macular degeneration in humans which, in most cases, leads to legal blindness by young adulthood. In 2001, Kang Zhang (Zhang et al., 2001), followed by Albert Edwards (Edwards et al., 2001) identified a new mutation in a previously unidentified human gene that they determined was responsible for the macular degeneration phenotype observed in STGD3 patients (Fig. 1). At the time of this discovery, the function of the gene in question was not known, but it was identified on human chromosome 6q14 and was shown to be highly conserved evolutionarily. Zhang named the gene ***ELO**ngation of **V**ery **L**ong chain fatty acids like-**4*** (*ELOVL4*) because of its sequence homology with a yeast family of proteins involved in the elongation of very long chain fatty acids (Zhang et al., 2003). The ELOVL family of elongases are responsible for performing the initial rate-limiting condensation reaction between an acyl-CoA and malonyl-CoA, resulting in a 3-ketoacyl-CoA that is further processed via a series of reduction and dehydration reactions to produce a fatty acid that is two carbons longer (Sassa and Kihara, 2014). ELOVL4 contains 314 amino acids with a calculated molecular weight of 36.8 kDa (Mandal et al., 2004; Zhang et al., 2003) and, in the retina, is highly enriched in the retinal rod and cone photoreceptors, and is concentrated in photoreceptor inner segments (Fig. 2A). Both Zhang and Edwards identified a 5-bp deletion (797–801_delAACTT) in exon 6 of *ELOVL4* that results in pre-mature termination and truncation of the wild-type protein (Edwards et al., 2001; Zhang et al., 2001). Later in 2001, Paul Bernstein (Bernstein et al., 2001) described a second mutation in *ELOVL4* as being responsible for another variation of familial STGD3. This mutation was two 1-bp deletions separated by four nucleotides (790delT+794delT) that resulted in a similar frameshift mutation in exon 6 and truncation of the wild-type protein. In 2004, Alessandra Maugeri (Maugeri et al., 2004) identified and described a third mutation in a European family with yet another variant of STGD3. This mutation was a heterozygous nonsense transversion (c.810C > G) within exon 6 of the *ELOVL4* gene, which resulted in a stop codon substitution for tyrosine 270 (p.Tyr270X). Again, the net result was a truncation of 45 amino acids from the WT ELOVL4 protein. This mutation has recently been reported in a Swiss family with STGD3 (Tran et al., 2016) that is not related to the Belgian family reported by Maugeri. In 2016, Bardak et al. (2016), reported two genetic variants in exon 6 in a Turkish family with the Stargardt-like disease phenotype. These variants include c.814G > C (p. E272Q) and c.895A > G (p. M299V) and may further confirm the link between STGD3 and ELOVL4. Most recently, Donato et al. reported a case of a 42-year-old Caucasian patient with dominant STGD phenotype that is associated with two *ELOVL4*

promoter variants, c. −236 C > T (rs240307) and c. −90 G > C (rs62407622) (Donato et al., 2018b). They showed that expression of the single c. −90 G > C or c. −236 C > T variants, as well as co-expression of the two variants (c.−90 G > C and c. −236 C > T), cause downregulation of ELOVL4 expression, based on reduced luciferase activity.

All of the mutations of *ELOVL4* in exon 6 that have been defined so far result in the loss of a C-terminal endoplasmic reticulum (ER) targeting sequence (KXKXX) required for the retention of *trans*-membrane proteins in the ER (Jackson et al., 1990, 1993; Zhang et al., 2001), the site of fatty acid elongation. Therefore, if produced, the mutant ELOVL4 protein would most likely be mislocalized. Initial *in vitro* studies confirmed this but gave conflicting results over the nature of the mislocalization. The first set of experiments conducted in African green monkey fibroblast-like cells (COS-7) and Chinese Hamster Ovary (CHO) cell lines demonstrated wild-type ELOVL4 localization to the ER, but expression of both mutations (5-bp and two 1-bp deletions) led to mislocalization from the ER to a scattered Golgi distribution (Ambasudhan et al., 2004). The second *in vitro* study using a recombinant N-terminal tagged Enhanced Green Fluorescent Protein-ELOVL4 (EGFP-ELOVL4) fusion approach evaluated the 5-bp deletion in NIH3T3 fibroblast and transformed human embryonic kidney (HEK283T) cell lines and reported a similar ER retention of the wild-type enzyme, but a mislocalization of the mutant enzyme to the cytoplasm in an aggregated pattern (Karan et al., 2004). Expression of a fluorescent-tagged version of the fourth mutation (p.Tyr270X) in NIH3T3 cells also suggested that the mutant ELOVL4 clustered as aggregates in the cytosol instead of being retained in the ER where the wild-type ELOVL4 enzyme localized (Maugeri et al., 2004). One possibility for the discrepancy in mutant ELOVL4 localization described in the first two studies (Ambasudhan et al., 2004; Karan et al., 2004) is the use of different cell lines. However, Grayson and Molday addressed this question using both COS-7 and HEK293T cells and found that expression of mutant 5-bp deleted *ELOVL4* in both cells lines resulted in an aggregated cytosolic mislocalization rather than being redistributed to the Golgi body (Grayson and Molday, 2005). Importantly, this study also demonstrated that co-expression of wild-type ELOVL4 with the 5-bp deleted mutant ELOVL4 resulted in a sequestration of the wild-type protein into these cytosolic aggresome-like inclusion bodies. Two follow-up studies confirmed this dominant negative effect, demonstrating that the C-terminally truncated mutant ELOVL4 recruits the wild-type ELOVL4 protein into cytosolic aggresomes and away from its intended ER target (Karan et al., 2005b; Vasireddy et al., 2005) and further, that mutant ELOLV4 expression may initiate an ER stress response via upregulation of the unfolded protein response (UPR) (Karan et al., 2004). Highlighting the relevance of such a molecular mechanism in the etiopathogenesis of retinal dystrophies such as STGD3, Donato et al. (2018a) recently described altered expression of several genes, as well as non-coding regulative RNA (e.g. miRNAs) following oxidative RPE stress and upregulation of the UPR. A later study of this dominant negative phenomenon suggested that truncated mutant ELOLV4 is also able to form hetero-oligomeric interactions with other fatty acid elongases, suggesting that it may alter other aspects of the fatty acid elongation pathway (Okuda et al., 2010).

2. Identification of the biological function of the ELOVL4 as a fatty acid elongase

In 2008, we discovered the function of ELOVL4 as a fatty acid elongase (Agbaga et al., 2008) necessary for biosynthesis of both saturated and polyunsaturated very long chain fatty acids (VLC-FA). We showed that expression of the mouse ELOVL4, using recombinant adenovirus type 5 viral particles carrying the mouse *Elovl4* minigene in both neonatal rat cardiomyocytes and immortalized human retinal pigment epithelial (ARPE-19) cells, resulted in the biosynthesis of VLC-FA (Agbaga et al., 2008) (Fig. 2B), which we define as a fatty acid with 28 or more carbon atoms. This study unequivocally demonstrated that ELOVL4 is able to synthesize both VLC-saturated (VLC-SFA) and VLC-polyunsaturated (VLC-PUFA) fatty acids. The precursor 26:0, a long chain (LC-FA) fatty acid, was elongated to both 28:0 and 30:0. The LC-PUFA eicosapentaenoic acid (20:5n3, EPA) and docosapentaenoic acid (22:5n3, DPA) were also elongated to a series of C28-C38 carbon VLC-PUFA (Agbaga et al., 2008) (Fig. 2C), with 20:5n3 being the preferred substrate for VLC-PUFA formation over both arachidonic acid (20:4n6, AA) and docosahexaenoic acid (22:6n3, DHA) (Yu et al., 2012). Importantly, we also demonstrated that ELOVL4 is not involved in the elongation of shorter chain 18:3n3 or 22:5n3 precursors to DHA (Agbaga et al., 2010a), another fatty acid that has been shown to be of critical importance in cellular function (Bazan, 2005, 2009; 2013; Bazan et al., 2011; Benolken et al., 1973; Crawford, 1970, 1976; Crawford et al., 2013; Kenchegowda et al., 2013; Lukiw et al., 2005; Mukherjee et al., 2004; Musto et al., 2011; Wheeler et al., 1975). In support of the evidence against a role for ELOVL4 in DHA biosynthesis, our lab demonstrated that enrichment of retinal DHA in *fat-1* transgenic mice expressing mutant ELOVL4 was not sufficient to protect against retinal degeneration *in vivo* (Li et al., 2009). This is supported by recent studies from Bernstein's group showing that clinical intervention with dietary fish oil supplements at a daily dose of 650 mg EPA and 350 mg DHA (NCT00420602) in STGD3 patients did not attenuate progression of maculopathy (Choi et al., 2018). These findings strongly support the hypothesis that progression of retinal pathology in STGD3 is most likely due to depletion of retinal VLC-FA synthesized by the ELOVL4 (Fig. 3A). Due to the exceptional length of the various VLC-FA made by ELOVL4, they are able to contribute unique biophysical properties to the cellular membranes that incorporate them, due to the number of methylene-interrupted *cis* double bonds within the acyl chain. The more saturated the chain (VLC-SFA), the more wax-like and rigid the membrane becomes (Hopiavuori et al., 2017b), while the more unsaturated the chain (VLC-PUFA), the more oil-like and fluid the membrane becomes (Ben Gedalya et al., 2009). However, given the critical role of DHA in retina function, the potential for some physiological benefit by DHA supplementation in human patients should not be ignored based on these studies alone.

In retinal tissues, the predominant VLC-FA are VLC-PUFA, which are incorporated into the *sn-1* position in phosphatidylcholine (PC) with DHA in the *sn-2* position (Fig. 3B). This unique combination provides fluid-like properties to the lipid bilayer. In bovine retina, VLC-PUFA are enriched in rod photoreceptor outer segments (OS) (Aveldano, 1987; Aveldano and Sprecher, 1987; Martin et al., 2005), as well as in both large ribbon synapses and smaller conventional synapses (Bennett et al., 2014b; Hopiavuori et al., 2016). The increased

fluidity of OS membranes, in part due to their high VLC-PUFA content, is favorable and may assist in photoreceptor disc migration and OS shedding to the retina pigment epithelium (RPE). The logic here is that VLC-PUFA can be described as longer versions of DHA, and therefore share its biophysical properties within a membrane. DHA, due to the presence of six methylene-interrupted *cis* double bonds (Dratz et al., 1985), imposes increased permeability, compression, fusion, flipping, and fluidity that improves membrane trafficking and signaling (Stillwell et al., 2005; Stillwell and Wassall, 2003; Wassall and Stillwell, 2008). Despite the lower relative concentration of VLC-PUFA in OS compared to DHA, the exceptional length and degree of unsaturation would make VLC-PUFA able to potentially impose a greater influence on membrane biophysical properties at lower abundance compared to shorter PUFA.

In the skin, the predominant VLC-FA are VLC-SFA incorporated into complex ω-O-acylceramides (Fig. 3C) that are condensed into the epidermal lamellar membranes (Elias and Wakefield, 2014) and serve as both necessary and sufficient components of the stratum corneum (Uchida and Holleran, 2008; Vasireddy et al., 2007), the epidermal barrier that prevents dehydration and protects skin and underlying tissues from the environment. (Uchida and Holleran, 2008; Vasireddy et al., 2007). This lipid was recently identified in retinal vasculature, where its long hairpin structure and VLC-SFA acyl chain were proposed to contribute to the integrity of the blood-retinal barrier by supporting membrane structure and stabilizing tight junctions due to its wax-like rigidity (Kady et al., 2018). In animal models of global VLC-SFA deficiency, mice die from excessive epidermal water loss within hours of birth due to the loss of VLC-SFA-containing ω-O-acylceramides (Li et al., 2007b; McMahon et al., 2007a; Uchida and Holleran, 2008; Vasireddy et al., 2007).

We recently reported that VLC-SFA are the predominant product of ELOVL4 in the central nervous system (CNS) (Hopiavuori et al., 2017b), as components of sphingolipids (Brush et al., 2010) (Fig. 3D). Our study demonstrated an enrichment of the VLC-SFA, 28:0 and 30:0, in synaptic vesicle membranes isolated from baboon hippocampus and identified a potentially critical role for ELOVL4 and VLC-FA in the brain in regulating vesicular exocytosis (Hopiavuori et al., 2017a, 2017b) that may hinge on the unique wax-like biophysical properties that VLC-SFA impose on a membrane bilayer (adapted in Fig. 9G).

3. Characteristics of the ELOVL4 protein

The ELOVL4 enzyme contains three distinct motifs within its protein sequence (Grayson and Molday, 2005): **1)** an N-glycosylation consensus motif at the N-terminus, **2)** a conserved catalytic histidine core (HVYHH), and **3)** an ER retention/retrieval motif (KAKGD) (Fig. 4). We assessed the role of each of these motifs in the fatty acid elongation process in a series of experiments using site-specific mutations of each of the motifs and determined their expression, localization, and fatty acid biosynthetic ability in ARPE-19, HEK293T, and HeLa cells (Logan et al., 2014). Our results demonstrate conclusively that *in vitro* enzymatic activity of ELOVL4 is dependent on both the catalytic histidine core as well as on the ER retention/retrieval signal, while mutation of the N-glycosylation consensus motif did not cause any change in enzymatic functionality (Logan et al., 2014) (Fig. 5). This suggested that in addition to being mislocalized, the mutant ELOVL4 is likely devoid of any

enzymatic activity. We tested this hypothesis using both cell-based and cell-free microsomal assays and demonstrated that the 5-bp deletion mutant ELOVL4 is enzymatically inactive, lacking all innate condensation activity (Logan et al., 2014). When co-expressed with wild-type ELOVL4, the mutant ELOVL4 also downregulated the wild-type ELOVL4 function, resulting in reduced VLC-PUFA synthesis *in vitro* (Logan et al., 2013). This dominant negative effect was predicted from the studies discussed earlier by Grayson and Molday, which showed a sequestration of wild-type ELOVL4 by mutant ELOVL4 into cytosolic aggresomes not associated with endoplasmic reticulum. Effectively, our studies rule out the possibility of a functionally active mutant enzyme (5-bp deletion) capable of synthesizing toxic ketone intermediates in the case of mutants lacking an ER retention motif. We went a step further and tested if restoring the ER retention motif to the mutant ELOVL4 (mutant-ELOVL4-ER) would restore enzyme activity. Although the mutant-ELOVL4-ER protein re-localized to the ER, the enzyme was still devoid of any condensation activity (Logan et al., 2013) (Fig. 6). These studies suggest that apart from a C-terminal ER motif, there are critical amino acids or structural elements within the missing 51 amino acids that are deleted in the 5bp mutant-ELOVL4 that are essential for the proper function of ELOVL4. It also left open the possibility that either loss of ELOVL4's VLC-PUFA products or the presence of a non-functional mutant ELOVL4 protein was causing cellular stress and subsequent photoreceptor death in STGD3 patients, or that a combination of these two scenarios contribute to STGD3 pathology. These questions could only be answered *in vivo* using appropriate animal models.

4. The conflict: *in vivo* models of Stargardt-like macular dystrophy and ELOVL4 deficiency

As the study of ELOVL4 and its various STGD3 mutations moved into animals, several different animals models were generated (see complete chronological list in Table 1) that told conflicting stories as to whether or not the STGD3 pathogenesis was the result of VLC-PUFA deficiency or the presence of a stress-inducing mutant ELOVL4 protein misplaced in the cytosol. It is important to mention here that murine models, which do not have a macula and are composed of ~95% rod photoreceptors are likely very limited in their ability to model macular pathology in humans. Furthermore, the use of different antibodies to track proteins, such as ELOVL4, is a likely source of discrepancy between the various findings on localization reported by the different groups using the models described in this review.

The first animal model was described in 2005 by Kang Zhang's group (Karan et al., 2005a), who made the initial mutant *ELOVL4* connection to human STGD3 disease (Zhang et al., 2001). This model was a transgenic (TG) mouse in which the human interphotoreceptor retinoid-binding protein (*IRBP)* promoter was used to drive expression of either the human wild-type *ELOVL4* mini-gene or the human 5-bp deletion *STGD3* mutant (790–794 AACTT) in mouse photoreceptors (Karan et al., 2005a). This mouse model(s) contained the two endogenous wild-type copies of *Elovl4* and over-expressed the human *STGD3* mutation at increasing copy numbers (TG1^{+}-, TG2^{+}-, TG3^{+}-mice from lowest to highest copy number), with human WT1 serving as a control (Karan et al., 2005a). The animals expressing mutant *ELOVL4* developed a profound and rapid retinal

degeneration resulting in retinal outer nuclear layer (ONL) cell loss, reduction in both a-max and b-max amplitudes in their ERG, and severe ultrastructural pathology with disorganized photoreceptor outer segments and large accumulations of lipofuscin and A2E (Karan et al., 2005a). The magnitude of the pathology described increased in severity in response to increasing transgene copy number of the human STGD3 mutation. The control human wild-type *ELOVL4* mini-gene transgenic constructs (WT1) showed no aberrant effects on retinal function in these mice (Karan et al., 2005a), although its level of expression differed from that of the mutated proteins. These studies suggest the mutant ELOVL4 contributes to retinal degeneration. However, the relationship between rate of retinal degeneration and copy number of the mutant *ELOVL4* transgene also suggests that the retinal degeneration could be due to over-expression of the mutant *ELOVL4* transgene. Several groups have shown that over-expression in photoreceptor cells of proteins such rhodopsin (wild type) can cause a retinal degeneration in mice (Wen et al., 2009). This issue still needs to be resolved.

Subsequent generation of *Elovl4* knock-out mice heterozygous for a null allele (*Elovl4*^{+/−}) were reported by two independent groups to be unremarkable with normal retinal morphology and function even up to 22 months of age, indicating that haploinsufficiency was not part of the underlying pathology in the mouse model of STGD3 (Li et al., 2007a; Raz-Prag et al., 2006).

In 2006, Vasireddy et al. generated a heterozygous knock-in model (*Elovl4*^{wt/mut}) by targeting the 5-bp deletion (AACTT) in the mouse *Elovl4* (Vasireddy et al., 2006). They reported a progressive photoreceptor degeneration with cone and RPE ultrastructural abnormalities detected as early as two months of age and rod involvement by 10 months of age. They also describe lower *Elovl4* mRNA levels but significantly higher expression of ELOVL4 in the inner segments and outer plexiform layer with enhanced dark- and light-adapted responses via electroretinography at both 8 and 15 months of age. Additionally, they reported significant reduction in 20:5, 22:5, and 24:6, none of which would turn out to be synthesized by ELOVL4. In fact, as the function of ELOVL4 had not yet been described, this study only included fatty acid comparisons up to a length of C24, which are precursors rather than products of ELOVL4 (Agbaga et al., 2008; Yu et al., 2012). A subsequent study of this mouse model up to 22 months of age by the same group described accumulation of dense lipofuscin granules in the RPE as well as an accumulation of ELOVL4 in the OPL, co-localizing with the bipolar dendritic marker, PKC-α (Vasireddy et al., 2009); retinal function was not evaluated in this study.

To further study the retinas of heterozygous 5-bp deletion mutant knock-in mice, McMahon et al. (2007a), generated an independent version of the mutant *Elovl4* knock-in mice (*Elovl4*^{wt/stgd3}) via targeted knock-in of the 5-bp deletion in the mouse *Elovl4* gene. This model was different from the *Elovl4*^{wt/mut} reported by Vasireddy et al. (2006) in that in addition to knocking in the 5-bp deletion, McMahon also included two downstream single nucleotide substitutions that resulted in a truncated mutant ELOVL4 protein containing 8 amino acids at the C-terminus that are identical to the protein product coded by one of the human pathogenic alleles (McMahon et al., 2007a; Zhang et al., 2001). Characterization of this second *stgd3* knock-in mouse revealed that at 1 month of age, wild-type *Elovl4* mRNA did not change as a consequence of the mutation and rather than enhanced ERG responses,

they described a significant reduction in both rod a-max and b-max values at 8 months of age, without a statistically significant reduction in cone response (McMahon et al., 2007a). Furthermore, in contrast to the progressive, early onset retinal degeneration described by Vasireddy (Vasireddy et al., 2006), there was no evidence for any morphological changes in these heterozygous mutant mice compared to littermate controls (McMahon et al., 2007a). This study, however, confirmed the observation (Vasireddy et al., 2006) of the presence of lipofuscin and accumulation of A2E precursors, but not of A2E itself, in the eyes of heterozygous *stgd3* mutant mice. A follow-up study by McMahon et al. reported that in contrast to earlier *in vitro* evidence for the up-regulation of the UPR by expression of the STGD3 mutation (Karan et al., 2004), they did not find any evidence for this type of cellular stress response *in vivo*, measured in the retinas of their mice heterozygous for the mutation (McMahon et al., 2007b). Lipidomic analysis of retinas from these mice did not find any significant loss of the long chain polyunsaturated fatty acids (LC-PUFA; C20–24) that are normally enriched in the vertebrate retina. However, they demonstrated a selective deficiency of C32-C36 polyunsaturated acyl phosphatidylcholines (McMahon et al., 2007b), which are now confirmed products of ELOVL4 (Agbaga et al., 2008). The group concluded from this evidence that *in vivo*, it is the deficit in these VLC-PUFA products and not cellular stress due to expression of a mutant enzyme that leads to the pathology in humans with STGD3 (McMahon et al., 2007b).

In 2011, Sommer et al. reported the generation of a transgenic pig as a large animal model for Stargardt-like macular dystrophy (Sommer et al., 2011). Due to the presence of the area centralis in pigs, which contains a cone-enriched region for heightened visual acuity, their rationale as that unlike the rod-dominant mouse, this would be a more representative model for human macular disease. The two mutation models generated were for the 5-bp deletion (797–801_delAACTT) and for the tyrosine pre-mature stop (Y270terEYFP), both using the rhodopsin Rho4.4 photoreceptor-specific promoter. The EYFP fusion peptide was used for histological visualization of the mutant ELOVL4 in the Tyr270X model. The study evaluated histological and functional (ERG) endpoints and reported mislocalization of the mutant ELOVL4 from the photoreceptor IS to the OS membranes, while causing disorganization of the photoreceptors and ONL layers of the retina (Sommer et al., 2011). Functionally, both models (5-bp del; n = 1/Y270terEYFP; n = 2) demonstrated diminished b-wave responses.

We subsequently attempted to reconcile the differences between the murine STGD3 animal models (Mandal et al., 2014). We assessed all three genetically modified mutant ELOVL4 mice: TG1$^+$ and TG2$^+$ mice (Karan et al., 2005a), *Elovl4$^{+/mut}$* heterozygous knock-in mice (Vasireddy et al., 2006, 2009), and *Elovl4$^{+/-}$* heterozygous knock-out mice (Raz-Prag et al., 2006). We determined ELOVL4 expression levels, localization, and products at 8–10 weeks of age using appropriate littermate controls for each transgenic line. In support of McMahon's reports (McMahon et al., 2007a, 2007b), we found a significant reduction in VLC-PUFA levels in *Elovl4$^{+/mut}$* retinas (~50% of littermate controls); a similar loss of VLC-PUFA was found in *Elovl4$^{+/-}$* but not in TG2$^+$ retinas, indicating that the presence of the mutant human ELOVL4 does not downregulate activity of the wild-type mouse enzyme (both copies present for TG2$^+$ mice) (Mandal et al., 2014). Using an antibody that recognized the wild-type but not the truncated mutant form of ELOVL4 (Agbaga et al., 2008), we also showed a marked reduction in ELOVL4 signal intensity in both *Elovl4$^{+/-}$*

and *Elovl4^(+/mut)* mouse retinas (Mandal et al., 2014), but did not detect any change in localization or accumulation of the ELOVL4 protein in the OPL, as previously described by others (Vasireddy et al., 2009). One possibility for this discrepancy may derive from differences in antibody specificity. In the study describing accumulation of ELOVL4 in the OPL of *Elovl4^(+/mut)* retinas, Vasireddy used an antibody that recognizes both the wild-type and mutant version of the protein and they did not find any ELOVL4 (which would presumably have been mutant) in the photoreceptor OS (Vasireddy et al., 2009).

To help resolve the differences in photoreceptor localization of the mutant ELOVL4 *in vivo*, we performed a series of molecular experiments in *Xenopus laevis* rod photoreceptors by expressing haemagglutinin (HA)-tagged murine ELOVL4 variants (Agbaga et al., 2014) (Fig. 7). We demonstrated unequivocally **1)** that in *X. laevis* photoreceptor cells, the mutant ELOVL4 lacking an ER retention motif is misrouted to the photoreceptor OS (not into the OPL and neural retina) and **2)** that adding the missing ER retention sequence to mutant ELOVL4 constructs restored wild-type IS localization of the mutant ELOVL4 protein (Agbaga et al., 2014), similar to what was described *in vitro* (Logan et al., 2013, 2014). This result, along with the mislocalization noted above for transgenic pigs, show that the shed tips of OS membranes likely contain mutant ELOVL4. Indeed, in 2015, Suavé's group (Kuny et al., 2015) evaluated RPE morphology, function (c-wave), and phagosome localization in the TG1–2 mouse line and found that the presence of the human ELOVL4 mutation (5bp-del. *STGD3*) in photoreceptors of TG1–2 mice leads to RPE cytotoxicity with a build-up of phagosomes on the apical side of the RPE cells, even at P30 just prior to the loss of photoreceptors and retinal function. The presence of the mutant protein led to defective processing of the disc outer segments by the RPE, which could induce cellular stress thereby contributing to understanding the underlying pathology seen in humans with STGD3. Their follow-up study (Dejos et al., 2018) using the same TG1–2 mouse model attempted to further identify the RPE dysfunction that is induced by the *STGD3* mutation expressed by photoreceptors. OS from mutant TG1–2 photoreceptors were fed to human RPE cells *in vitro* and the kinetics of phagocytosis was determined using a pulse-chase experimental design. The results of this study demonstrated that there is early pathology detected in RPE cells as well as in microglia/macrophages when exposed to the human 5bp mutant ELOVL4. These *in vitro* studies revealed a delay in the degradation of OS membranes by RPE. At the peak of OS uptake by RPE cells, they found a 50% reduction in the abundance of acidified RPE phagolysosomes *in vivo*, prior to any signs of retinal degeneration. In these TG1–2 mice, they found evidence that this processing delay (observed at P30) involves **1)** increased expression of the crystalline protein and lysosomal regulator, CRYBA1/A3, **2)** upregulation of the drusen component CRYBB2, and **3)** invasion of microglia/macrophage to the retina. In a recent study, David William's group (Esteve-Rudd et al., 2018) honed in on the molecular mechanism responsible for the delayed phagocytosis of human mutant ELOVL4 by the RPE. After confirming mislocalization of the mutant ELOVL4 to the OS in the TG2 mouse model, they conducted a pulse-chase experience *in vitro* in which they fed OS from TG2 mice to primary RPE cells cultured from both TG2 mice and WT controls. After normal ingestion of the mutant OS by the primary RPE cells (Esteve-Rudd et al., 2018), they confirmed inefficient processing of those OS membranes by the RPE and demonstrated that this was due to excessive sequestration of both RAB7A and dynein to the mutant

phagosomes. They conclude that due to this inefficient sequestration, RPE phagosomes are defective in both recruiting and utilizing the appropriate motor linkers necessary for apical to basal migration to the endolysosomes for degradation. These findings suggest that the underlying pathology in STGD3 may be at least in part due to RPE inefficiency in digesting phagolysosomes that contain mutant ELOVL4. The effect on RPE survival and long-term function needs to be determined.

Global homozygous expression of the *Elovl4* mutations or knockout of *Elovl4* gene results in neonatal lethality due to dehydration (Li et al., 2007a; McMahon et al., 2007a; Raz-Prag et al., 2006; Vasireddy et al., 2007). To circumvent this defect in order to understand the impact of retinal VLC-PUFA depletion in the absence of any mutation, three different conditional knock-out (cKO) mouse lines have been generated using a Cre-lox approach (Bennett et al., 2014b; Harkewicz et al., 2012). Harkewicz et al. (2012) reported the functional consequences of either rod- or cone-specific conditional deletion of *Elovl4* on retinal function and health in mice. Analysis of these lines demonstrated that *Elovl4* deletion from rods resulted in a greater loss of VLC-PUFA, especially of those C32 than was seen following *Elovl4* deletion from cones, which fits with the reported enrichment of the VLC-PUFA in rod OS disc membranes (Anderson and Maude, 1970; Aveldano and Sprecher, 1987; Brush et al., 2010). At 3–5 months of age there was no evidence for any morphological or structural abnormalities relative to controls except for some age-dependent loss of rod photoreceptor cells in the rod-cKO line. Functionally, the rod-cKO demonstrated a significant functional (ERG) reduction in the scotopic b-max response as well as in the mixed b-max response, while cone cKO mice demonstrated a significant reduction in photopic flicker response (Harkewicz et al., 2012).

A second pair of conditional rod- or cone-specific deletions were generated and described by Barabas et al. (2013). The first Cre line (*Opsin-Cre*) for rod-specific deletion of *Elovl4* was the same line used in the prior study by Harkewicz (Harkewicz et al., 2012), but was reported here to be an incomplete deletion of the ELOVL4 protein, with some rods still expressing the wild-type enzyme, resulting in only a 58% reduction in total retinal VLC-PUFA levels (Barabas et al., 2013). In contrast to the previous report on these mice (Harkewicz et al., 2012), Barabas et al., did not detect any functional reduction in scotopic or photopic ERG responses in any of their described cKO lines (rod-cKO1, rod-cKO2, cone cKO) up to 10 months of age (Barabas et al., 2013), twice the age at which Harkewicz describes a 25–45% reduction in both rod and cone b-wave responses (Harkewicz et al., 2012). They followed this finding by generating a second rod-cKO2 line using the *Opsin-iCre75*, which resulted in 89% total reduction in *Elovl4* mRNA and a 98% reduction in retinal VLC-PUFA (Barabas et al., 2013). Still, however, they did not find any evidence for reduction in ERG function up to 10 months of age in these rod-cKO2 animals and proposed that the remaining 2% VLC-PUFA may be sufficient to produce a functional retina, but also strongly concluded that VLC-PUFA do not play an important role in photoreceptor function or survival. However, it should be pointed out that the *Opsin-iCre75* Cre-driver does not begin to excise floxed genomic DNA in murine rods until post-natal day 7 (P7) and does not result in complete excision until P18 (Li et al., 2005). Since *Elovl4* expression (Mandal et al., 2004; Zhang et al., 2003) begins at E7 to E15, it is possible that Barabas' rod-cKO mice had sufficient levels of VLC-PUFA at a time when they were important in retinal

structure and function. The cone cKO mouse described therein did not demonstrate any significant change in VLC-PUFA levels and none of the cKO lines showed any evidence for morphological changes, including photoreceptor degeneration (Barabas et al., 2013). This study also compared their KO findings with paired studies of Karan's TG[+] animals that express the human *STGD3* cDNA as a transgene driven by the human *IRBP* promoter. They confirm the same rapid degeneration in these animals and the same functional ERG deficits (Barabas et al., 2013) following STGD3 over-expression. They also describe a significant loss of VLC-PUFA in the TG[+] retinas with an additional loss of DHA by 7 months of age. ELOVL4 is not involved in the DHA synthesis pathway (Agbaga et al., 2010a), and therefore the reduction in VLC-PUFA (and DHA) seen in their study is almost certainly a consequence of the severe photoreceptor degeneration seen in these animals (e.g. by 7 months of age there is nearly complete loss of the photoreceptor cells). This study also ruled out any significant upregulation of the UPR response in TG[+] retinas, confirming a previous report (McMahon et al., 2007b). However, in line with known responses in retinal degenerations, there was a significant upregulation in the activated astrocyte marker, GFAP (Barabas et al., 2013). TG[+] mice still have both functional wild-type copies of ELOVL4 and therefore retain VLC-PUFA synthetic ability. VLC-PUFA and DHA are paired in PC in photoreceptor OS (Brush et al., 2010), so it would be expected to see a time-dependent loss of both with progressive death of these cells. A later study confirmed that at 10 weeks of age, the human *STGD3* mutation is not capable of exerting a dominant negative effect on the murine wild-type enzyme to reduce VLC-PUFA levels (Mandal et al., 2014) *in vivo*. Therefore, it had been proposed by Barabas and others that in light of the absence of any significant cone degeneration in these animals, the TG[+] mice, despite serving as an excellent model for rapid photoreceptor degeneration, may not be a representative model of the human disease. It is possible that overexpression of a non-endogenous mutant human transgene and subsequent misrouting to the outer segments (Agbaga et al., 2014) is in itself causing retinal degeneration due to the sheer magnitude of the cellular stress this places on the RPE as a consequence of an overwhelming amount of mutant protein being included in its daily phagocytic OS load. Indeed, Kuny et al. (2015) demonstrated in Karan's TG[+] animals that expression of the human STGD3 mutant protein in the mouse photoreceptor causes signs of RPE toxicity prior to any signs of photoreceptor loss and made the observation that abnormal clearance of the photoreceptor outer segments by the RPE may be a fundamental cause of the rod outer segment truncation and photoreceptor death observed in these animals (Dejos et al., 2018; Kuny et al., 2010, 2012, 2014, 2015). This is not an unfamiliar concept, since over-expressing P23H mutant forms of the rhodopsin as a transgene causes rapid and progressive photoreceptor degeneration in mice (Goto et al., 1995; Olsson et al., 1992). However, it is important to note that one critical difference between the P23H mice and the TG[+] mice is that the P23H mutation is misrouted to the ER and as a consequence, the photoreceptors do demonstrate an increased UPR response indicating ER stress (Liu et al., 1996), whereas the TG[+] mice do not (Barabas et al., 2013; McMahon et al., 2007b).

Recently, our group tested the importance of VLC-FA on retinal function using conditional deletion of *Elovl4* from all photoreceptors (Bennett et al., 2014a, 2014b). An important difference in this model of VLC-FA deficiency was the use of a *Chx10-Cre* mice (Jackson Laboratories, Bar Habor, Maine) crossed to *Elovl4*[flox/flox] mice (Rowan and Cepko, 2004)

to conditionally delete ELOVL4 from rods and cones at a time before the *Elovl4* gene is expressed in these cells. The *Chx10* gene is expressed in neural progenitor cells briefly during embryonic development (E9.5-E16.5) (Liu et al., 1994), which overlaps with onset of *Elovl4* expression (E7–E15) in retina (Mandal et al., 2004), resulting in efficient CRE-mediated deletion of *Elovl4* from the neural retina (including photoreceptors) prior to wild-type expression. Importantly, since *Chx10* is turned off by E16.5 (retained by only a subset of bipolar cells), this model controls well for any negative consequences of constitutive CRE expression within the photoreceptors and thus avoids OS build-up of a non-endogenous cytosolic protein. *Elovl4* deletion was confirmed with a 91% reduction in mRNA and 96% reduction in protein (Bennett et al., 2014a). Protein expression was determined using a previously published and validated antibody that recognizes the wild-type but not truncated mutant versions of ELOVL4 (Agbaga et al., 2008). Retinal levels of DHA or any other < C26 fatty acid were not affected by retinal *Elovl4* deletion; however, fatty acid species > C26 were barely detectable in *Chx10*-cKO retinas and those levels were further reduced from 8 weeks to 12 months of age (Bennett et al., 2014a). Retinal function in these mice was evaluated using ERG at 5 weeks and 12 months of age. At 5 weeks there was no effect of *Elovl4* deletion on rod responses, but at 12 months of age there was a marked reduction in both a- and b-wave mediated rod responses. The VLC-FA deficient *Chx10*-cKO mice had a 22% reduction in maximum rod response amplitude compared to wild-type and heterozygous littermate controls (controlled for *Cre* expression). Further dissection of the scotopic b-wave response assessed both maximum bipolar response amplitude (V_{max}) and the implicit time (IT) of the maximum b-wave amplitude achieved within the response. At 12 months of age, *Chx10*-cKO mice had a 32% lower V_{max}, a 16.9 ms delay in intrinsic time (IT), and a significant reduction in the b/a-wave ratio compared to wild-type littermates. In contrast to the rod-cKO1 mice (Barabas et al., 2013; Harkewicz et al., 2012) that lost only 58% of the total retinal VLC-PUFA and allowed nearly 29 days of wild-type *Elovl4* expression before complete excision from rod photoreceptors, the 12-month-old *Chx10-cKO* mice had a significant loss of rod photoreceptors (Bennett et al., 2014a). In support of Barabas' findings in their cone-cKO mouse (Barabas et al., 2013), cone structure and function in *Chx10*-cKO mice was not significantly different from controls (Bennett et al., 2014a). Taken together, these results demonstrate that loss of VLC-PUFA causes an age-dependent reduction in rod photoreceptor function and survival, but not in cones of mice. Thus, while accumulation of mutant protein may affect events in the RPE, these studies, in which neither wild type nor mutant ELOVL4 are expressed, clearly demonstrate an effect of the absence of VLC-PUFA on rod structure and function.

Given the substantial loss of b-wave responses in the retinas of 12 month old *Chx10*-cKO mice, a subsequent study of these animals (Bennett et al., 2014b) was done to further decipher the effect of VLC-FA deficiency on retinal function. This study measured inner retina function via ERG, synaptic connectivity, and ultrastructural changes within photoreceptor terminals of VLC-FA deficient *Chx10-cKO* mice. They described a significant reduction of rod-mediated a- and b-wave responses in VLC-FA deficient mice. Oscillatory potential (OP) wavelets, considered to originate from feedback responses sent between the amacrine, horizontal, and bipolar cells in response to the rod photoresponse (Wachtmeister, 1998), were quantified in 9-month-old *Chx10*-cKO mice and found to be significantly

lower in amplitude compared to controls. The power density of the OP response was also significantly lower in *Chx10*-cKO mice, although frequency and latency of the OP response was not. This would suggest that VLC-PUFA may also be playing an important role in synaptic function of the neural retina. Indeed, Bennett et al. demonstrated that VLC-PUFA concentrations are significantly enriched within both large ribbon synaptosomes made up of connections between photoreceptors and bipolar cells as well as within the smaller conventional synaptosomes isolated from the neural retina (Bennett et al., 2014b). Whole cell patch clamp studies in retinal slices isolated from wild-type and *Chx10*-cKO mice revealed that the deficits in retinal synaptic signaling do not derive from defective rod pre-synaptic voltage-gated calcium currents (I_{Ca}) or rod-bipolar cell post-synaptic glutamate currents. Additionally, *Chx10*-cKO mice revealed synaptic reorganization at both 9 and 12 months of age with a marked disruption of both ONL and OPL expression patterns. This indicates that depletion of VLC-PUFA may cause changes in the membrane structure of pre-synaptic photoreceptor terminals, causing them to withdraw into the ONL and away from the bipolar cell dendrites, resulting in subsequent disruption of synaptic organization within the OPL. This phenomenon causing disruption of the OPL could be what Vasireddy et al. (2009) indirectly observed and interpreted as accumulation of ELOVL4 in the OPL of their knock-in mice heterozygous for the 5-bp deletion mutant ELOVL4, possibly due to some unexpected off-target labeling of the retracting terminals by the antibody used in that study. Ultrastructural analysis of VLC-FA deficient photoreceptor terminals via transmission electron microscopy (TEM) revealed a reduction in both synaptic vesicle number and diameter in rod pre-synaptic terminals, suggesting that at least some aspect of the abnormal synaptic activity in the retina may be mediated by altered pre-synaptic transmission due to dysregulation of pre-synaptic vesicle structure and/or function.

These studies suggest that the products of ELOVL4 play an important role in photoreceptor function due to their relatively high concentration in PC in OS. VLC-FA may also be playing an important role in the synaptic function of rod photoreceptors within the neural retina. This notion is expanded and supported by our brain studies discussed in the next section.

5. The expanding physiological and clinical relevance of ELOVL4 and VLC-FA: focus on central nervous system

Since its discovery, ELOVL4's VLC-FA products have been described as components of several other more complex lipid molecules with tissue-specific distribution. ELOVL4 synthesizes VLC-PUFA in the retina (Agbaga et al., 2008) as components of phosphatidylcholine (PC) enriched in photoreceptor outer segments (Aveldano, 1987) and in testes as components of sphingolipids (Brush et al., 2010; Poulos et al., 1987). ELOVL4 synthesizes VLC-SFA that are incorporated into several sphingolipids including unique (*O*-acyl)-ω-hydroxyl fatty acids that have been unequivocally determined to provide the epidermal water barrier in the skin (Cameron et al., 2007; Li et al., 2007b; McMahon et al., 2007a, 2011; Vasireddy et al., 2007) and contribute to the tear film in the Meibomian gland (McMahon et al., 2014).

The first clinical study to describe mutations in *ELOVL4* as responsible for a severe neuro-ichthyotic disease in humans was reported by Aldahmesh et al. (2011), who identified homozygous inheritance of two novel recessive truncating mutations in *ELOVl4* in children [c.646C > T (p.Arg216X) in exon 5] and [c.690del (p.Ile230Metfs*22) in exon 6]. These children were described as having severe ichthyosis, intellectual disability, delayed myelination, brain atrophy, spastic quadriplegia, and violent seizures, and died within the first decade of life. Interestingly, the macula of these children appeared normal without any evidence for retinal deficits; however, these children died around the time that vison loss associated with autosomal dominant Stargardt's disease begins (Bernstein et al., 2001; Edwards et al., 2001; Zhang et al., 2001).

Another case report of homozygous inheritance was published in 2014 and described a second novel, recessive nonsense mutation in *ELOVL4* [c.78C > G (p.Tyr26*)] in exon 1 in human patients presenting with another neuro-ichthyotic disorder with variable expression (Mir et al., 2014). This mutation was the first described in the N-terminus of the ELOVL4 protein and is predicted to lack protein expression due to either nonsense mediated mRNA decay or, as in the other cases, via production of a truncated protein lacking all five transmembrane domains, the histidine active site, and the dilysine ER retention motif. The resulting phenotype in these patients was variable in that the severity of erythematous ichthyosis and CNS involvement was not equal between the three affected individuals. One of the affected family members demonstrated a profound developmental delay with severe seizures beginning in the first year of life. The frequency of these seizures was high, occurring at 20 min intervals. Both upper and lower extremities displayed hallmarks of severe hypertonia with extreme weakness noted in both bone and muscle. Interestingly, this individual also displayed significant dental erosion, although to date, involvement of ELOVL4 in the development of calcified tissues such as bone and teeth has not been evaluated. This individual was 16 years old at the time of the study, but died a year later. Mortality has not been reported in the other two affected individuals, who were 22 and 24 years old at the time of the study. Interestingly, there was no report of macular degeneration in these patients.

In 2014, Cadieux-Dion et al. (2014) reported a French Canadian family with an autosomal dominant mutation in *ELOVL4* and spinocerebellar ataxia-34 (SCA34) and erythrokeratodermia variabilis (EKV). The novel heterozygous transversion mutation described in this study [c.540G > C (p.L168F) in exon 4] was reported to result in a severe EKV beginning at infancy, but in most cases disappearing by 25 years of age (Cadieux-Dion et al., 2014). SCA34 onset was detected within the fourth and fifth decade of life (mean age of onset = 51 years) and slowly progressed. Mild peripheral neuropathy was also described in half of the affected individuals, suggesting a possible role for ELOVL4 within the peripheral nervous system as well (PNS). MRI scans showed severe cerebellar atrophy.

Additional case studies in 2015 added to the list of *ELOVL4* mutations causing CNS involvement in humans. One study described yet another novel heterozygous mutation in *ELOVL4* [c.736T > G (p.W246G) in exon 6] causing SCA34 with the hot cross bun sign (cruciform hyperintensity with axial T2-weighted MRI images) with progressive gait and limb ataxia with dysarthria in 100% of affected individuals (Ozaki et al., 2015); the mean

onset of SCA34 in this study was 34 years of age and was progressive. Contrary to other *ELOVL4* mutations that cause SCA34 (Bourassa et al., 2015; Cadieux-Dion et al., 2014), this study did not report any evidence for EKV. The third SCA mutation reported another novel heterozygous missense mutation in *ELOVL4* [c.539A > C (p.Gln180Pro) in exon 4] (Bourassa et al., 2015). This individual presented with a progressive gait disorder with erythematous skin lesions, which in combination were diagnosed as SCA34 with EKV. Ataxia began in the patient's mid-20s with evidence for both cerebellar and pontine atrophy on MRI at the time of this study in his 30s.

For a complete list of the ELOVL4 mutations described to date in humans, please see Table 2.

6. Understanding the role of ELOVL4 in the CNS; a shift to *in vivo* studies

Biallelic inheritance of mutant *ELOVL4* results in a severe neurodevelopmental phenotype in human children. These children develop severe seizures, intellectual disability, and pre-mature mortality within the first decade of life (Aldahmesh et al., 2011). The overarching limitation in trying to understand the underlying mechanism behind this profound neurological condition lies in the fact that global deletion or mutation of *Elovl4* results in neonatal lethality (Cameron et al., 2007; Li et al., 2007b; McMahon et al., 2007a, 2011; Vasireddy et al., 2007). In mice, *Elovl4* mRNA expression begins embryonically at E7 and is detectable in both brain and retina at P1, at which time expression increases in the retina and decreases in the brain until levels stabilize around P30 (Mandal et al., 2004). Homozygous mutation or deletion of *Elovl4* in mice is neonatal lethal due to the loss of (O-acyl)-ω-hydroxyl VLC-SFA from ceramides in the skin, which provide critical barrier and moisture-retaining functions (Cameron et al., 2007; Li et al., 2007b; McMahon et al., 2007a; Vasireddy et al., 2007). McMahon et al., demonstrated that targeting back wild-type *Elovl4* as a transgene under the skin-specific control of the *INVOLUCRIN* promoter is capable of rescuing levels of the VLC-SFA in the skin of homozygous 5-bp deletion mutation knock-in mice, subsequently rescuing the neonatal lethality (McMahon et al., 2011).

Our group developed a similar animal model, in which we generated homozygous 5-bp deletion mutant mouse knock-in mice that express wild-type *Elovl4* under control of *KERATIN-14* promoter. The *INVOLUCRIN*-skin-rescued animals were kindly provided to us by Wojciech Kedzierski, Ph.D. which allowed us to generate double $Tg^{K-14}Tg^{INV}$ (S^+) $Elovl4^{mut/mut}$ mice ($S^+Elovl4^{mut/mut}$). These $S^+Elovl4^{mut/mut}$ mice survived, but developed severe tonic-clonic seizures at P18–19 and died by P21 (Hopiavuori et al., 2017b), which is similar to the humans with homozygous mutations in ELOVL4, described in section 5 (Aldahmesh et al., 2011), who die within the first decade of life from a profound seizure disorder. Our attempts to uncover the link between ELOVL4 and these seizures lead us to identify an essential role for VLC-SFA in mammalian survival. We utilized loss of function and rescue approaches to identify the novel regulation of presynaptic neurotransmission in the mouse hippocampus by two ELOVL4-specific brain-derived VLC-SFA, 28:0 and 30:0.

In P20 mice, ELOVL4 is expressed in several different brain regions, with highest expression found within neurons of the cerebellum, thalamus, hippocampus, and cortex

(Hopiavuori et al., 2017b; Sherry et al., 2017) (Fig. 8A). In the hippocampus, a known locus for temporal medial lobe seizures (Navidhamidi et al., 2017; Soussi et al., 2015), ELOVL4 expression was very strong in CA3 and the polymorphic layer of the dentate gyrus (DG), as well as in the subiculum and entorhinal cortex, which provide synaptic input to the hippocampal circuit. The neurons to which DG projects in CA2 and CA1 regions showed weaker ELOVL4 labeling (Hopiavuori et al., 2017b; Sherry et al., 2017) (Fig. 8B). Neural imaging and biochemical approaches showed that biallelic inheritance of mutant ELOVL4 creates a high degree of metabolic stress on the brain. PET imaging revealed a 3-fold increase in fluorescein-labeled 2-deoxyglucose uptake (Fig. 8C–D) in the brains of $S^+Elovl4^{mut/mut}$ mice without blood brain barrier compromise determined by MRI with gadolinium, while metabolomics confirmed a 3-fold increase in ATP production, demonstrating highly increased energy demand.

We previously reported lipidomic analysis of all detectable glycerophospholipid molecules found in six different brain regions plus retina of the C57B6 mouse at 2, 10, and 26 months of age (Hopiavuori et al., 2017a). We identified two brain-derived VLC-SFA products of ELOVL4, 28:0 and 30:0 as components of sphingolipids. Furthermore, membrane fractionation and lipidomic analysis (Hopiavuori et al., 2017c) of freshly dissected baboon hippocampus revealed a dramatic enrichment of both 28:0 and 30:0 in synaptic vesicle membranes relative to the other membrane fractions analyzed (Hopiavuori et al., 2017b) (Fig. 9A–E). Although VLC-PUFA were abundant in retinal phosphatidylcholine, they were not detectable in the brain aside from a small single peak present during early embryogenesis that was too small to permit quantification (Hopiavuori et al., 2017a).

Our studies suggested a specialized role for VLC-SFA in the structural and/or functional integrity of synaptic vesicles in the brain. Indeed, FM1–43 dye studies revealed a loss of slow-releasing synapses in primary neuronal cultures harvested at E18.5 from $Elovl4^{mut/mut}$ and $Elovl4^{wt/wt}$ mice indicating that loss of the 28:0 and 30:0 VLC-SFA products from vesicle membranes resulted in a significant shift to the right in their release rate kinetics. This shift was not achieved by speeding up pre-synaptic neurotransmission in general, as the kinetics of all synapses were not changed, but rather by selective loss of what appeared to be a group of slow-releasing synapses. Recording of spontaneous extracellular hippocampal field potentials in $S^+Elovl4^{mut/mut}$ slices confirmed a burst-like firing pattern in these animals instead of the more sporadic, tonic firing patterns detected in wild-type littermate controls. This bursting activity could initiate spontaneous spreading epileptiform activity through the whole hippocampus under physiologic conditions, as we observed intermittently in $S^+Elovl4^{mut/mut}$ slices (Fig. 8E). In addition, $S^+Elovl4^{mut/mut}$ mice demonstrated a significantly higher frequency of field excitatory postsynaptic potentials (fEPSP) during periods of spontaneous activity, but with a significant decrease in overall frequency and fEPSP amplitude for the recording. This may reflect inadequate spatial and/or temporal summation, which dictates the properties of a post-synaptic field potential generated by hippocampal neurons (Cash and Yuste, 1999; Hao et al., 2009; Poirazi et al., 2003a; b). The observed pattern of spontaneous activity may represent an uncoupling of the neuron's control over the timing and duration of its spontaneous pre-synaptic release. VLC-SFA deficiency affects the probability of synchronized release events due to the loss of their proposed "braking" influence, which has the potential to provide a degree

of fine-tuning to release kinetics during vesicle fusion. Loss of this braking system, and therefore the means for this tight temporal regulation of vesicle release, could result in a net dysregulation of spatial and temporal summation within VLC-SFA deficient synapses by reducing the occurrence of spatial/temporal summation down to a probability event instead of a tightly controlled signaling process. Ultimately, we postulate that as a function of time the probability that these erratic pre-synaptic burst-responses will eventually synchronize increases, and when they do, achieve a degree of temporal and spatial summation that is large enough to initiate epileptogenic activity. We tested this idea by artificially elevating the probability of release by global depolarization (7.5 mM K^+ ACSF) in both $S^+Elovl4^{mut/mut}$ mice and their wild-type littermate controls, thereby ensuring that maximal pre-synaptic release rates could occur in both genotypes. This revealed that under strong depolarizing conditions, slices from $S^+Elovl4^{mut/mut}$ mice trend towards a higher frequency of fEPSP responses than wild-type littermate controls. In addition, $S^+Elovl4^{mut/mut}$ mice had a significantly higher amplitude in their field potentials under depolarizing conditions that increased in magnitude along the hippocampal tri-synaptic circuit, with DG showing the smallest magnitude change and CA1 showing the largest. This experiment supports the concept that the apparent absence of slow pre-synaptic release due to the absence of VLC-SFA results in a significantly larger magnitude response within the hippocampal circuit as a whole when synchronized pre-synaptic release is achieved in the brains of $S^+Elovl4^{mut/mut}$ mice compared to wild-type littermate controls.

To separate any pleiotropic effects of the genetic manipulation verus the absence of VLC-SFA products produced by ELOVL4, we supplemented neuronal cultures with an equimolar mixture of the two major ELOVL4 products in the brain (28:0 + 30:0) and with 24:0, a precursor for ELOVL4 elongation that is present in neurons of both genotypes, serving as a control LC-SFA. Supplementation of the $Elovl4^{mut/mut}$ cultures with 28:0 and 30:0 rescued synaptic release rates to wild-type levels, while release rates in 24:0-supplemented neuronal cultures were not corrected (Fig. 9F). These results suggest that it is indeed the absence of the VLC-SFA and not the presence of the mutant STGD3 ELOVL4 protein that is responsible for the pre-synaptic dysregulation in the brains of these animals.

The molecular mechanism by which VLC-SFA regulates the kinetics of pre-synaptic vesicle release is currently unknown. One attractive possibility is outlined in our present working model (Fig. 9G). Under normal conditions, VLC-SFAs exist in an amide linkage with a sphingolipid on one side of the lipid bilayer and, because of their length and the absence of any *cis* double bonds, can extend through the lipid bilayer and interact with fatty acyl chains esterified to glycerophospholipids and sphingolipids with polar head groups on the other side of the bilayer. We propose that such acyl-acyl hydrophobic interactions across the lipid bilayer would increase the van der Waals forces within the bilayer, thereby stabilizing the membranes and resisting fusion with other membranes. The absence of these interactions, which would occur with functional *Elovl4* depletion, could increase the probability of release events such as we observed in the current study via loss of this potential braking mechanism. These VLC-SFA in opposing leafs of the vesicle membrane could thereby provide a biophysical resistance capable of fine-tuning the timing of vesicle release independent of the calcium-driven activation of protein complexes, a machinery that is essential for Ca^{2+}-regulated release of synaptic vesicles (Deák et al., 2006, 2009; Imig

et al., 2014; Sudhof and Rizo, 2011; Südhof and Rothman, 2009; Zhou et al., 2015). This concept is supported in part by Rohrbough et al., where loss-of-function mutations in the *Drosophila* ceramidase gene, *slab*, resulted loss of readily releasable vesicles as shown by FM1–43 dye studies (Rohrbough et al., 2004). Subsequent EM of synapses isolated from these flies revealed a significant increase of synaptic vesicles linked together and tethered at the plasma membrane, but unable to fuse. Ceramidase enzymes are responsible for cleaving esterified fatty acids from molecules with a sphingosine backbone (El Bawab et al., 2002). In brain tissue, this class of enzymes demonstrated a significantly higher cleavage preference for longer chain saturated fatty acids and monounsaturated fatty acids than for shorter chain or polyunsaturated ones (El Bawab et al., 2002). All of ELOVL4's products that we identified in the brain were found within the sphingosine-based classes of lipid. In support of our findings, we propose that due to the absence of *slab* ceramidase in the Rohrbough study, *Drosophila* neurons were unable to cleave these very long chain saturated fatty acids from the sphingosine molecules contained in synaptic vesicle membranes. Esterification and cleavage biochemistry can happen in a rapid and non-genomic manner. Constant regulation of the concentration of these very long chain saturated fatty acids within synaptic vesicle membranes by ongoing cleavage and esterification of different length acyl-chains would allow for a secondary braking mechanism capable of using biophysical properties to fine-tune pre-synaptic signaling; the higher the concentration of VLC-SFA, the more rigid and less fusible synaptic vesicle membranes will be.

Alternatively, the length and saturation of VLC-SFA may enable them to sterically inhibit protein-protein interactions in the vesicular release machinery. However, interactions between VLC-SFA and the vesicle fusion machinery remain unknown at present.

Our study of ELOVL4 in the brain (Hopiavuori et al., 2017b) advances the knowledge of synaptic physiology relating to synaptic vesicle endo- and exocytosis, providing direct evidence that: 1) VLC-SFA are highly enriched in the pre-synaptic vesicle membranes of a non-human primate (baboon) relative to other neuronal membranes (Hopiavuori et al., 2017b), 2) absence of VLC-SFA alters the rate of presynaptic vesicle release, and critically, 3) VLC-SFA supplementation rescues mutant synapses back to normal release rates (Hopiavuori et al., 2017b). With this understanding, future studies to identify the mechanistic targets could provide improved therapies for epilepsy and other neurological disorders. This work established a connection between VLC-SFA and epileptiform seizures (Hopiavuori et al., 2017b), but the specific nature of this relationship must still be resolved.

In tying these findings in brain back to the retina, we have proposed the hypothesis that the loss of synaptic vesicle number and changes in structural morphology in *Chx10-cKO* mice (Bennett et al., 2014b) is likely a consequence of VLC-FA deficiency in these specialized membranes (Hopiavuori et al., 2016). This hypothesis is supported in part by a recent report (Donato et al., 2018b) showing that expression of the c.−90 G > C or c. −236 C > T variants, and co-expression of the c. −90 G > C and c. −236 C > T ELOVL4 variants, in the promoter region of ELOVL4, cause downregulation of ELOVL4 activity. Furthermore, changes to pre-synaptic fusion dynamics in the retina via loss of either VLC-PUFA from photoreceptor pre-synaptic terminals or from the presynaptic terminals of other neurons within the neural retina could explain the large differences observed in the various dissected components of

the ERG response in *Chx10-cKO* mice (Bennett et al., 2014b). VLC-PUFA share the same biophysical properties as DHA, but are able to impose a greater influence on membrane fluidity due to their exceptional length (Agbaga et al., 2010b). Enrichment of VLC-PUFA in synaptic vesicle membranes could drive a significant increase in presynaptic vesicle pool turnover. Indeed, FM1–43 dye studies (Ben Gedalya et al., 2009) reveal that incubation of neuronal cells with PUFA of various length and degrees of unsaturation, results in a quantitative increase in FM1–43 signal internalization compared to Bovine Serum Albumin (BSA) controls, which directly corresponds to both the length and degree of unsaturation of the LC-PUFA added. The authors reported that the longer and more polyunsaturated the fatty acid was, the more FM1–43 dye accumulated in the endocytic vesicles within the cell (Ben Gedalya et al., 2009). Cork et al. (2016), recently published some very interesting findings that demonstrate the presence of miniature excitatory post-synaptic currents (mEPSCs) in the horizontal cells of tiger salamander retina, in the absence of any exocytosis-driving stimulus. Furthermore, they demonstrate that although blocking Ca^{2+} reduced the frequency of these mEPSCs, it did not eliminate them. This demonstrates that mEPSCs can occur independently of any Ca^{2+} present to drive vesicle fusion machinery. It is a fascinating possibility that simply enriching the amount of PUFA content of a vesicle membrane as a function of both the length and degree of unsaturation could produce synaptic vesicles with membranes so fluid that they are able to fuse and drive post-synaptic currents independent of any protein machinery to facilitate that fusion. In a neuronal network such as the retina, where depolarization is the constant, it would be evolutionarily favorable for these types of perpetually active synapses to incorporate high levels of PUFA, LC-PUFA, and VLC-PUFA into their vesicle membranes in order to reduce the energy demands associated with Ca^{2+}-dependent exocytosis. In the study reported by Bennett et al. (2014), there was no significant difference in ICa^{2+} between WT and *Chx10-cKO* mice, indicating that loss of presynaptic ICa^{2+} is not responsible for any decreases in synaptic transmission in *Chx10-cKO* mice. Post-synaptic glutamatergic currents mediated by mGluR6 were measured and no significant differences were detected between WT and *Chx10-cKO* mice, indicating that changes in the b-wave were not mediated by dysregulation of post-synaptic glutamate currents. A lack of significant differences between WT and *Chx10-cKO* mice in both pre-synaptic ICa^{2+} and postsynaptic rod bipolar cell glutamate receptor currents indicates that the decrease in synaptic transmission is most likely due to deficits in pre-synaptic release downstream of ICa^{2+}, but upstream of post-synaptic metabotropic glutamate receptor responses (Hopiavuori et al., 2016). A critical observation is that the diameters of synaptic vesicles from *Chx10-cKO* mice were significantly smaller than those from WT mice, 24.5 nm vs. 29.5 nm, respectively (Bennett et al., 2014b). Because volume scales with the cube of radius, this relatively small change in diameter would result in a reduction in volume, and thus glutamate content, of ~57%–43% of control. This reduction in glutamate content may explain the 50% decrease in b-wave amplitude in *Chx10-cKO* mice (Bennett et al., 2014b; Hopiavuori et al., 2016). Therefore, it is likely that the decreased presynaptic vesicle size and number resulted in decreased synaptic efficiency and drove the reorganization of the rod terminals and the bipolar dendrites within the OPL, as was observed (Bennett et al., 2014b).

It would appear, on the surface, that we are arguing that due to their exceptional length, VLC-FA are able to either biophysically stabilize membranes in their saturated forms due to the presence of long, wax-like acyl chains, or biophysically destabilize membranes due to the presence of 5 and 6 methylene interrupted *cis* double bonds that allow for rapid flux between various states of torsion, driving increased membrane permeability, fusion, and flipping (Hasadsri et al., 2013; Stillwell et al., 2005; Stillwell and Wassall, 2003). In other words, each of these types of molecules have highly unique biophysical properties that would drastically alter membrane properties based on their degree of unsaturation, even at low endogenous concentrations, due to their unique lengths and membrane packing characteristics. Therefore, it is reasonable that some membranes could use VLC-SFA in sphingolipids to stabilize and regulate synaptic vesicle fusion, whereas other neural cell functions would rely on the VLC-PUFA in phospholipids for the fluidityinducing properties they bring to synaptic membranes that might enable the rapid transmission of synaptic information.

7. Discovery of a new class of bioactive VLC lipid-derivatives: elovanoids as novel neuroprotectants

Work recently published by Nicolas Bazan's group (Bhattacharjee et al., 2017; Jun et al., 2017) describes the discovery of cell-specific, dihydroxylated derivatives of n-3 VLC-PUFA they named "Elovanoids" (ELVs) (Fig. 10). These bioactive derivatives of C32 VLC-PUFA (ELV-N32) (Fig. 10D) or C34 VLC-PUFA (ELV-N34) (Fig. 10G) are produced as a paracrine/autocrine pro-homeostatic response by human RPE cells to serve a protective function in those cells that are undergoing uncompensated oxidative stress (UOS) (Jun et al., 2017). They propose an alternative benefit for VLC-PUFA content in the retina and further reinforce the importance of these molecules in mediating RPE and photoreceptor health for the maintenance of mammalian vision. This may also explain the age-dependent phenotype we observed (Bennett et al., 2014a, 2014b), that over the course of the animal's lifetime any reduction in ELOVL4 would translate to less VLC-PUFA available in the photoreceptor outer segments and therefore RPE, to protect against oxidative stress and ultimately to support retinal and RPE function.

Of further interest, Bazan's group also described the presence of these molecules in the CNS and demonstrated their endogenous prohomeostatic ability to protect neuronal cells against **1)** uncompensated oxidative stress, **2)** oxygen/glucose deprivation as one would observe during ischemia/stroke, and **3)** *N*-methyl-D-aspartate (NMDA) receptor-mediated excitotoxicity, as one would observe during an epileptic seizure and other neurological disorders (Bhattacharjee et al., 2017). These findings provide critical, additional insights into the potential mechanism behind the devastating seizures and death observed in both mice and humans with bi-allelic mutations in ELOVL4 (Aldahmesh et al., 2011; Hopiavuori et al., 2017b). VLC-SFA regulation of synaptic vesicle fusion kinetics and the neuroprotective role of ELVs generate new questions about the multifaceted roles that ELOVL4, VLC-FA, and now, their bioactive ELV derivatives are playing to support the health and function of mammalian nervous tissues.

It is important to note here, that ELVs as well as other bioactive neuroprotectants like the DHA-derived NPD1 (Bazan, 2005), can be synthesized and provided exogenously to study their effects on cellular function, but are unable to be quantified in tissues endogenously. As of now, there are no obvious avenues available to test the hypothesis of whether the content of ELVs may be altered or regulated by a disease state *in vivo*.

8. A conundrum: how can different mutations in the same gene lead to such different phenotypes (Stargardt-like macular dystrophy vs. spinocerebellar ataxia)?

There are really two issues here. The first is how does the wildtype ELOVL4 synthesize VLC-PUFA in retina and testes and VLC-SFA in brain, skin, and Meibomian glands? The second is how do the different mutations cause the different phenotypes? With regard to the first issue, it is possible that local factors specific to the cells expressing ELOVL4 influence the substrate specificity of the enzyme. We know nothing about potential binding partners of ELOVL4 in different cells. ELOVL4 is one of four microsomal enzymes necessary for the addition of a 2-carbon unit to a C26 fatty acid. There could be tissue specificity in any one of the other three enzymes that could select for either SFA or PUFA. We do know that the tissue specificity is not in ELOVL4, since it synthesizes both VLC-SFA and VLC-PUFA when expressed in cell culture (Agbaga et al., 2008). Also, the availability of SFA vs. PUFA precursors can also influence the products that are formed. For example, skin and Meibomian glands have very little PUFA, so the available C26 precursor is saturated and the VLC-FA product is VLC-SFA. Likewise, the retina and the testes have large amounts of PUFA, so their production of VLC-PUFA is understandable. However, the brain is the wild card here. In spite of having widespread expression of ELOVL4 (Fig. 8) and large amounts of PUFA (Hopiavuori et al., 2017a), we have not been able to find any VLC-PUFA in PC (Hopiavuori et al., 2017a) or sphingolipids (Brush et al., 2010). Likewise, the VLC-SFA we find are concentrated in sphingolipids in synaptic vesicles (Hopiavuori et al., 2017b). Bazan (personal communication) suggests that VLC-PUFA are synthesized in small amounts locally and utilized immediately for the synthesis of Elovanoids and have no function as a structural lipid in the brain. We tend to agree with this since we do not find VLC-PUFA in any membrane lipid in the brain.

One other possibility that we have not sufficiently addressed is the role of the N-glycosylation site in regulating substrate availability and product formation. We know that site specific mutations within the N-glycosylation site are not required for condensation activity in the synthesis of VLC-PUFA (Logan et al., 2014). However, none of the three cell lines used (ARPE-19, HEK293T, and HeLa) endogenously express ELOVL4. It has been shown that N-glycosylation sites are utilized by cell-specific glycan structures that vary depending on the tissues that make them (Berger et al., 2016). An alternative hypothesis that must be tested is whether these different mutations affect the glycan structures that can access the N-glycosylation site on ELOVL4 in a cell-specific manner and influence the VLC-FA that are synthesized. Furthermore, very little is known about other potential post-translational modification sites or the types of epigenetics that may regulate ELOVL4.

There is indirect evidence that ELOVL4 may be regulated by epigenetic methylation in other disease states, as was reported for pancreatic adenocarcinoma (Omura et al., 2008).

The second issue is how different mutations in the same gene (*ELOVL4*) can cause such drastically different phenotypes in humans (Table 2). We must keep in mind that these different phenotypes occur in tissues expressing one mutant and one wild type copy of the ELOVL4. We know that in mammals, the same ELOVL4 enzyme synthesizes two types of fatty acids (VLC-PUFA and VLC-SFA) that vary drastically in their biophysical properties and in the tissue specificity. We have hypothesized that the different ELOVL4 mutations described throughout this review can affect the activity of the enzyme in one of several ways (Agbaga, 2016): **1)** Each specific mutation may uniquely affect the biosynthesis of either VLC-PUFA or VLC-SFA, so that mutations causing CNS and skin disorders may affect the synthesis of VLC-SFA without having any effect on the synthesis of VLC-PUFA. We have preliminary unpublished results that support this notion. We generated a knock-in rat that expresses one of the SCA34 mutations discussed earlier and found that the homozygous mutant offspring survived and had a full retinal complement of VLC-PUFA, but significantly reduced VLC-SFA in skin lipids (and subsequent skin pathology). **2)** The dominant negative effect of mutant ELOVL4 on the wild-type ELOVL4 may of itself be capable of influencing the type of VLC-FA produced. We know from our earlier studies that the enzymatic activity of wild type ELOVL4 for VLC-PUFA synthesis is inhibited in tissue culture by the STGD3 (5 bp deletion) mutant protein (Logan et al., 2013). We did not determine if the STDG3 ELOVL4 affected the synthesis of VLC-SFA. Current ongoing studies in our lab are directed towards determining if the mutant protein (STGD3 vs. SCA34) influences the products produced by the wild type ELOVL4.

9. Concluding remarks & future directions

We can state unequivocally that very long chain fatty acids are necessary for life. Their complete absence in humans leads to severe somatic and nervous system disorders that cause extreme morbidity and early death. Without VLC-SFA, rodents die at birth. Heterozygous expression of ELOVL4 also leads to human diseases such as Stargardt-like macular dystrophy, spinocerebellar ataxia, and erythrokeratodermia which, although not fatal, nevertheless are severely debilitating and take a toll on the quality of life, especially in an aging population. Therefore, we propose that VLC-FA be added to the family of "essential fatty acids" that are necessary for sustaining a number of important bodily functions that are essential for maintaining optimal human health and happiness. Furthermore, due to the monogenetic nature of these ELOVL4-associated disorders, it would be prudent to develop gene-therapy strategies to target functional ELOVL4 back to the deficient tissue. This would be especially important for the children with ELOVL4-associated macular degeneration, as there has already been some success in the clinic with gene therapy for retina disease.

Since VLC-FA occur naturally, it seems logical to assume that they would be readily available for human consumption. However, this is not the case. While VLC-SFA are readily available and can be prepared from a variety of waxes such as beeswax, by their biophysical nature, they are very solid at room temperature and cannot be emulsified and absorbed by the intestine. We are currently developing methods for the derivatization and packaging of

VLC-SFA so that they can be absorbed by the intestine and delivered to target tissues. The VLC-PUFA present another problem, as so far they have only been found in large amounts (relative to other fatty acids) in retina and sperm, neither of which is a source for human consumption. Very low levels of VLC-PUFA are present in some fish oils, but to date no fish oil concentrate containing VLC-PUFA is commercially available. Chemical synthesis has thus far been difficult and expensive.

Market forces can drive the commercial production of VLC-FA products in at least important four areas: macular degeneration, dry eye, dry skin, and male infertility. While STGD3 may be considered an orphan disease, age-related macular degeneration (AMD) certainly is not. Bernstein's lab (Choi et al., 2018; Liu et al., 2013) has shown that donor retinas from AMD patients have lower levels of VLC-PUFA than retinas from age-matched non-AMD donors. Since AMD is a major cause of new blindness in the aging population, VLC-PUFA supplements may be of some benefit in slowing down or preventing development of AMD in susceptible patients.

Dry eye is a huge problem that causes significant morbidity in humans of all ages. One cause is the absence or reduction of the lipid tear film that prevents evaporation of tears. Finding a way to supply VLC-SFA derivatives in eye drops or in implantable devices could provide an effective treatment of dry eye.

Loss of VLC-SFA in the skin is also a key hallmark of atopic dermatitis (Elias, 2014; Elias and Wakefield, 2014; Park et al., 2012), which is the most common chronic inflammatory skin disorder (Weidinger and Novak, 2016) affecting 20% of all children and 3% of adults worldwide (Asher et al., 2006). This is due to their critical role as precursors to the synthesis of ω-O-acylceramides, the key epidermal barrier lipid (Cameron et al., 2007; Jennemann et al., 2012; Li et al., 2007b; McMahon et al., 2007a, 2011; Ohno, 2017; Uchida and Holleran, 2008; Vasireddy et al., 2007) that protects the epidermis from the external environment. Development of topical products that can deliver VLC-SFA derivatives to underlying cells of the skin could provide an effective treatment of dry skin.

Absence of VLC-PUFA in mouse testes results in infertility. Zadravec et al. (2011) showed that deletion of *Elovl2*, the enzyme that converts C-22 PUFA to C-24/26 PUFA (precursors of VLC-PUFA), resulted in mouse male infertility (Zadravec et al., 2011). In these mice, providing DHA did not restore fertility, indicating that DHA itself cannot cure fertility. There is a large literature showing correlations with DHA and sperm motility, most likely reflective of its conversion to VLC-PUFA. In a large patient population study (n = 155) (Zerbinati et al., 2016), the seminal fluid level of DHA was positively correlated (r = 0.65) with sperm motility. We have unpublished results showing a very high positive correlation (p < 0.0001) between VLC-PUFA in sperm sphingomyelin and sperm motility and count. It is likely that some forms of male infertility could be effectively treated with oral supplementation of VLC-PUFA.

Acknowledgments

References

Agbaga MP, 2016. Different mutations in ELOVL4 affect very long chain fatty acid biosynthesis to cause variable neurological disorders in humans. Adv. Exp. Med. Biol 854, 129–135. [PubMed: 26427403]

Agbaga MP, Brush RS, Mandal MN, Elliott MH, Al-Ubaidi MR, Anderson RE, 2010a. Role of Elovl4 protein in the biosynthesis of docosahexaenoic acid. Adv. Exp. Med. Biol 664, 233–242. [PubMed: 20238022]

Agbaga MP, Brush RS, Mandal MN, Henry K, Elliott MH, Anderson RE, 2008. Role of Stargardt-3 macular dystrophy protein (ELOVL4) in the biosynthesis of very long chain fatty acids. Proc. Natl. Acad. Sci. U.S.A 105, 12843–12848. [PubMed: 18728184]

Agbaga MP, Mandal MN, Anderson RE, 2010b. Retinal very long-chain PUFAs: new insights from studies on ELOVL4 protein. J. Lipid Res 51, 1624–1642. [PubMed: 20299492]

Agbaga MP, Tam BM, Wong JS, Yang LL, Anderson RE, Moritz OL, 2014. Mutant ELOVL4 that causes autosomal dominant stargardt-3 macular dystrophy is misrouted to rod outer segment disks. Investig. Ophthalmol. Vis. Sci 55, 3669–3680. [PubMed: 24833735]

Aldahmesh MA, Mohamed JY, Alkuraya HS, Verma IC, Puri RD, Alaiya AA, Rizzo WB, Alkuraya FS, 2011. Recessive mutations in ELOVL4 cause ichthyosis, intellectual disability, and spastic quadriplegia. Am. J. Hum. Genet 89, 745–750. [PubMed: 22100072]

Ambasudhan R, Wang X, Jablonski MM, Thompson DA, Lagali PS, Wong PW, Sieving PA, Ayyagari R, 2004. Atrophic macular degeneration mutations in ELOVL4 result in the intracellular misrouting of the protein. Genomics 83, 615–625. [PubMed: 15028284]

Anderson RE, Maude MB, 1970. Phospholipids of bovine outer segments. Biochemistry 9, 3624–3628. [PubMed: 5509846]

Asher MI, Montefort S, Bjorksten B, Lai CK, Strachan DP, Weiland SK, Williams H, Group IPTS, 2006. Worldwide time trends in the prevalence of symptoms of asthma, allergic rhinoconjunctivitis, and eczema in childhood: ISAAC Phases One and Three repeat multicountry cross-sectional surveys. Lancet 368, 733–743. [PubMed: 16935684]

Aveldano MI, 1987. A novel group of very long chain polyenoic fatty acids in dipolyunsaturated phosphatidylcholines from vertebrate retina. J. Biol. Chem 262, 1172–1179. [PubMed: 3805015]

Aveldano MI, Sprecher H, 1987. Very long chain (C24 to C36) polyenoic fatty acids of the n-3 and n-6 series in dipolyunsaturated phosphatidylcholines from bovine retina. J. Biol. Chem 262, 1180–1186. [PubMed: 3805016]

Barabas P, Liu A, Xing W, Chen CK, Tong Z, Watt CB, Jones BW, Bernstein PS, Krizaj D, 2013. Role of ELOVL4 and very-long-chain polyunsaturated fatty acids in mouse models of Stargardt type 3 retinal degeneration. Proc. Natl. Acad. Sci. U.S.A 110, 5181–5186. [PubMed: 23479632]

Bardak H, Gunay M, Ercalik Y, Bardak Y, Ozbas H, Bagci O, Ayata A, Sonmez M, Alagoz C, 2016. Analysis of ELOVL4 and PRPH2 genes in Turkish Stargardt disease patients. Genet. Mol. Res : GMR 15.

Bazan NG, 2005. Neuroprotectin D1 (NPD1): a DHA-derived mediator that protects brain and retina against cell injury-induced oxidative stress. Brain Pathol 15, 159–166. [PubMed: 15912889]

Bazan NG, 2009. Neuroprotectin D1-mediated anti-inflammatory and survival signaling in stroke, retinal degenerations, and Alzheimer's disease. J. Lipid Res 50 (Suppl. l), S400–S405. [PubMed: 19018037]

Bazan NG, 2013. The docosanoid neuroprotectin D1 induces homeostatic regulation of neuroinflammation and cell survival. Prostaglandins Leukot. Essent. Fatty Acids 88, 127–129. [PubMed: 23022417]

Bazan NG, Musto AE, Knott EJ, 2011. Endogenous signaling by omega-3 docosahexaenoic acid-derived mediators sustains homeostatic synaptic and circuitry integrity. Mol. Neurobiol 44, 216–222. [PubMed: 21918832]

Ben Gedalya T, Loeb V, Israeli E, Altschuler Y, Selkoe DJ, Sharon R, 2009. Alphasynuclein and polyunsaturated fatty acids promote clathrin-mediated endocytosis and synaptic vesicle recycling. Traffic 10, 218–234. [PubMed: 18980610]

Bennett LD, Brush RS, Chan M, Lydic TA, Reese K, Reid GE, Busik JV, Elliott MH, Anderson RE, 2014a. Effect of reduced retinal VLC-PUFA on rod and cone photoreceptors. Investig. Ophthalmol. Vis. Sci 55, 3150–3157. [PubMed: 24722693]

Bennett LD, Hopiavuori BR, Brush RS, Chan M, Van Hook MJ, Thoreson WB, Anderson RE, 2014b. Examination of VLC-PUFA-deficient photoreceptor terminals. Investig. Ophthalmol. Vis. Sci 55, 4063–4072. [PubMed: 24764063]

Benolken RM, Anderson RE, Wheeler TG, 1973. Membrane fatty acids associated with the electrical response in visual excitation. Science 182, 1253–1254. [PubMed: 4752217]

Berger RP, Dookwah M, Steet R, Dalton S, 2016. Glycosylation and stem cells: regulatory roles and application of iPSCs in the study of glycosylation-related disorders. Bioessays 38, 1255–1265. [PubMed: 27667795]

Bernstein PS, Tammur J, Singh N, Hutchinson A, Dixon M, Pappas CM, Zabriskie NA, Zhang K, Petrukhin K, Leppert M, Allikmets R, 2001. Diverse macular dystrophy phenotype caused by a novel complex mutation in the ELOVL4 gene. Investig. Ophthalmol. Vis. Sci 42, 3331–3336. [PubMed: 11726641]

Bhattacharjee S, Jun B, Belayev L, Heap J, Kautzmann MA, Obenaus A, Menghani H, Marcell SJ, Khoutorova L, Yang R, Petasis NA, Bazan NG, 2017. Elovanoids are a novel class of homeostatic lipid mediators that protect neural cell integrity upon injury. Sci. Adv 3, e1700735. [PubMed: 28959727]

Bourassa CV, Raskin S, Serafini S, Teive HA, Dion PA, Rouleau GA, 2015. A new ELOVL4 mutation in a case of spinocerebellar ataxia with erythrokeratodermia. JAMA Neurol 72, 942–943. [PubMed: 26258735]

Brush RS, Tran JT, Henry KR, McClellan ME, Elliott MH, Mandal MN, 2010. Retinal sphingolipids and their very-long-chain fatty acid-containing species. Investig. Ophthalmol. Vis. Sci 51, 4422–4431. [PubMed: 20393115]

Cadieux-Dion M, Turcotte-Gauthier M, Noreau A, Martin C, Meloche C, Gravel M, Drouin CA, Rouleau GA, Nguyen DK, Cossette P, 2014. Expanding the clinical phenotype associated with ELOVL4 mutation: study of a large French-Canadian family with autosomal dominant spinocerebellar ataxia and erythrokeratodermia. JAMA Neurol 71, 470–475. [PubMed: 24566826]

Cameron DJ, Tong Z, Yang Z, Kaminoh J, Kamiyah S, Chen H, Zeng J, Chen Y, Luo L, Zhang K, 2007. Essential role of Elovl4 in very long chain fatty acid synthesis, skin permeability barrier function, and neonatal survival. Int. J. Biol. Sci 3, 111–119.

Cash S, Yuste R, 1999. Linear summation of excitatory inputs by CA1 pyramidal neurons. Neuron 22, 383–394. [PubMed: 10069343]

Choi R, Gorusupudi A, Bernstein PS, 2018. Long-term follow-up of autosomal dominant Stargardt macular dystrophy (STGD3) subjects enrolled in a fish oil supplement interventional trial. Ophthalmic Genet 39, 307–313. [PubMed: 29377748]

Cork KM, Van Hook MJ, Thoreson WB, 2016. Mechanisms, pools, and sites of spontaneous vesicle release at synapses of rod and cone photoreceptors. Eur. J. Neurosci 44 (3), 2015–2027. [PubMed: 27255664]

Crawford MA, 1970. The progression of long-chain fatty acids from herbivore to carnivore and the evolution of the nervous system. Biochem. J 119, 47P.

Crawford MA, 1976. Lipids and development of the human brain. Biochem. Soc. Trans 4, 231–233. [PubMed: 1001654]

Crawford MA, Broadhurst CL, Guest M, Nagar A, Wang Y, Ghebremeskel K, Schmidt WF, 2013. A quantum theory for the irreplaceable role of docosahexaenoic acid in neural cell signalling throughout evolution. Prostaglandins Leukot. Essent. Fatty Acids 88, 5–13. [PubMed: 23206328]

Deák F, Shin OH, Kavalali ET, Südhof TC, 2006. Structural determinants of synaptobrevin 2 function in synaptic vesicle fusion. J. Neurosci. : Off. J. Soc. Neurosci 26, 6668–6676.

Deák F, Xu Y, Chang WP, Dulubova I, Khvotchev M, Liu X, Südhof TC, Rizo J, 2009. Munc18–1 binding to the neuronal SNARE complex controls synaptic vesicle priming. J. Cell Biol 184, 751–764. [PubMed: 19255244]

Dejos C, Kuny S, Han WH, Capel H, Lemieux H, Sauve Y, 2018. Photoreceptor-induced RPE phagolysosomal maturation defects in Stargardt-like Maculopathy (STGD3). Sci. Rep 8, 5944. [PubMed: 29654292]

Donato L, Bramanti P, Scimone C, Rinaldi C, D'Angelo R, Sidoti A, 2018a. miRNAexpression profile of retinal pigment epithelial cells under oxidative stress conditions. FEBS Open Bio 8, 219–233.

Donato L, Scimone C, Rinaldi C, Aragona P, Briuglia S, D'Ascola A, D'Angelo R, Sidoti A, 2018b. Stargardt phenotype Associated with two ELOVL4 promoter variants and ELOVL4 downregulation: new possible perspective to etiopathogenesis? Investig. Ophthalmol. Vis. Sci 59, 843–857. [PubMed: 29417145]

Dratz EA, Van Breemen JF, Kamps KM, Keegstra W, Van Bruggen EF, 1985. Two-dimensional crystallization of bovine rhodopsin. Biochim. Biophys. Acta 832, 337–342. [PubMed: 4074754]

Edwards AO, Donoso LA, Ritter R 3rd, 2001. A novel gene for autosomal dominant Stargardt-like macular dystrophy with homology to the SUR4 protein family. Investig. Ophthalmol. Vis. Sci 42, 2652–2663. [PubMed: 11581213]

El Bawab S, Usta J, Roddy P, Szulc ZM, Bielawska A, Hannun YA, 2002. Substrate specificity of rat brain ceramidase. J. Lipid Res 43, 141–148. [PubMed: 11792733]

Elias PM, 2014. Lipid abnormalities and lipid-based repair strategies in atopic dermatitis. Biochim. Biophys. Acta 1841, 323–330. [PubMed: 24128970]

Elias PM, Wakefield JS, 2014. Mechanisms of abnormal lamellar body secretion and the dysfunctional skin barrier in patients with atopic dermatitis. J. Allergy Clin. Immunol 134, 781–791 e781. [PubMed: 25131691]

Esteve-Rudd J, Hazim RA, Diemer T, Paniagua AE, Volland S, Umapathy A, Williams DS, 2018. Defective phagosome motility and degradation in cell non-autonomous RPE pathogenesis of a dominant macular degeneration. Proc. Natl. Acad. Sci. U.S.A 115, 5468–5473. [PubMed: 29735674]

Goto Y, Peachey NS, Ripps H, Naash MI, 1995. Functional abnormalities in transgenic mice expressing a mutant rhodopsin gene. Investig. Ophthalmol. Vis. Sci 36, 62–71. [PubMed: 7822160]

Grayson C, Molday RS, 2005. Dominant negative mechanism underlies autosomal dominant Stargardt-like macular dystrophy linked to mutations in ELOVL4. J. Biol. Chem 280, 32521–32530. [PubMed: 16036915]

Hao J, Wang XD, Dan Y, Poo MM, Zhang XH, 2009. An arithmetic rule for spatial summation of excitatory and inhibitory inputs in pyramidal neurons. Proc. Natl. Acad. Sci. U.S.A 106, 21906–21911. [PubMed: 19955407]

Harkewicz R, Du H, Tong Z, Alkuraya H, Bedell M, Sun W, Wang X, Hsu YH, Esteve-Rudd J, Hughes G, Su Z, Zhang M, Lopes VS, Molday RS, Williams DS, Dennis EA, Zhang K, 2012. Essential role of ELOVL4 protein in very long chain fatty acid synthesis and retinal function. J. Biol. Chem 287, 11469–11480. [PubMed: 22199362]

Hasadsri L, Wang BH, Lee JV, Erdman JW, Llano DA, Barbey AK, Wszalek T, Sharrock MF, Wang HJ, 2013. Omega-3 fatty acids as a putative treatment for traumatic brain injury. J. Neurotrauma 30, 897–906. [PubMed: 23363551]

Hopiavuori BR, Agbaga MP, Brush RS, Sullivan MT, Sonntag WE, Anderson RE, 2017a. Regional changes in CNS and retinal glycerophospholipid profiles with age - a molecular blueprint. J. Lipid Res 58, 668–680. [PubMed: 28202633]

Hopiavuori BR, Bennett LD, Brush RS, Van Hook MJ, Thoreson WB, Anderson RE, 2016. Very long-chain fatty acids support synaptic structure and function in the mammalian retina. OCL 23, D113.

Hopiavuori BR, Deak F, Wilkerson JL, Brush RS, Rocha-Hopiavuori NA, Hopiavuori AR, Ozan KG, Sullivan MT, Wren JD, Georgescu C, Szweda L, Awasthi V, Towner R, Sherry DM, Anderson RE, Agbaga MP, 2017b. Homozygous expression of mutant ELOVL4 leads to seizures and death in a novel animal model of very long-chain fatty acid deficiency. Mol. Neurobiol 55 (2), 1795–1813. [PubMed: 29168048]

Hopiavuori BR, Masser DR, Wilkerson JL, Brush RS, Mandal NA, Anderson RE, Freeman WM, 2017c. Isolation of neuronal synaptic membranes by sucrose gradient centrifugation. Methods Mol. Biol 1609, 33–41. [PubMed: 28660571]

Imig C, Min SW, Krinner S, Arancillo M, Rosenmund C, Sudhof TC, Rhee J, Brose N, Cooper BH, 2014. The morphological and molecular nature of synaptic vesicle priming at presynaptic active zones. Neuron 84, 416–431. [PubMed: 25374362]

Jackson MR, Nilsson T, Peterson PA, 1990. Identification of a consensus motif for retention of transmembrane proteins in the endoplasmic reticulum. EMBO J 9, 3153–3162. [PubMed: 2120038]

Jackson MR, Nilsson T, Peterson PA, 1993. Retrieval of transmembrane proteins to the endoplasmic reticulum. J. Cell Biol 121, 317–333. [PubMed: 8468349]

Jennemann R, Rabionet M, Gorgas K, Epstein S, Dalpke A, Rothermel U, Bayerle A, van der Hoeven F, Imgrund S, Kirsch J, Nickel W, Willecke K, Riezman H, Grone HJ, Sandhoff R, 2012. Loss of ceramide synthase 3 causes lethal skin barrier disruption. Hum. Mol. Genet 21, 586–608. [PubMed: 22038835]

Jun B, Mukherjee PK, Asatryan A, Kautzmann MA, Heap J, Gordon WC, Bhattacharjee S, Yang R, Petasis NA, Bazan NG, 2017. Elovanoids are novel cell-specific lipid mediators necessary for neuroprotective signaling for photoreceptor cell integrity. Sci. Rep 7, 5279. [PubMed: 28706274]

Kady NM, Liu X, Lydic TA, Syed MH, Navitskaya S, Wang Q, Hammer SS, O'Reilly S, Huang C, Seregin SS, Amalfitano A, Chiodo VA, Boye SL, Hauswirth WW, Antonetti DA, Busik JV, 2018. ELOVL4-Mediated production of very long-chain ceramides stabilizes tight junctions and prevents diabetes-induced retinal vascular permeability. Diabetes 67, 769–781. [PubMed: 29362226]

Karan G, Lillo C, Yang Z, Cameron DJ, Locke KG, Zhao Y, Thirumalaichary S, Li C, Birch DG, Vollmer-Snarr HR, Williams DS, Zhang K, 2005a. Lipofuscin accumulation, abnormal electrophysiology, and photoreceptor degeneration in mutant ELOVL4 transgenic mice: a model for macular degeneration. Proc. Natl. Acad. Sci. U.S.A 102, 4164–4169. [PubMed: 15749821]

Karan G, Yang Z, Howes K, Zhao Y, Chen Y, Cameron DJ, Lin Y, Pearson E, Zhang K, 2005b. Loss of ER retention and sequestration of the wild-type ELOVL4 by Stargardt disease dominant negative mutants. Mol. Vis 11, 657–664. [PubMed: 16145543]

Karan G, Yang Z, Zhang K, 2004. Expression of wild type and mutant ELOVL4 in cell culture: subcellular localization and cell viability. Mol. Vis 10, 248–253. [PubMed: 15073583]

Kenchegowda S, He J, Bazan HE, 2013. Involvement of pigment epithelium-derived factor, docosahexaenoic acid and neuroprotectin D1 in corneal inflammation and nerve integrity after refractive surgery. Prostaglandins Leukot. Essent. Fatty Acids 88, 27–31. [PubMed: 22579364]

Kuny S, Cho WJ, Dimopoulos IS, Sauve Y, 2015. Early onset ultrastructural and functional defects in RPE and photoreceptors of a stargardt-like macular dystrophy (STGD3) transgenic mouse model. Invest. Ophthalmol. Vis. Sci 56, 7109–7121. [PubMed: 26529045]

Kuny S, Filion MA, Suh M, Gaillard F, Sauve Y, 2014. Long-term retinal cone survival and delayed alteration of the cone mosaic in a transgenic mouse model of stargardt-like dystrophy (STGD3). Invest. Ophthalmol. Vis. Sci 55, 424–439. [PubMed: 24334447]

Kuny S, Gaillard F, Mema SC, Freund PR, Zhang K, Macdonald IM, Sparrow JR, Sauve Y, 2010. Inner retina remodeling in a mouse model of stargardt-like macular dystrophy (STGD3). Investig. Ophthalmol. Vis. Sci 51, 2248–2262. [PubMed: 19933199]

Kuny S, Gaillard F, Sauve Y, 2012. Differential gene expression in eyecup and retina of a mouse model of Stargardt-like macular dystrophy (STGD3). Investig. Ophthalmol. Vis. Sci 53, 664–675. [PubMed: 22199241]

Li F, Marchette LD, Brush RS, Elliott MH, Le YZ, Henry KA, Anderson AG, Zhao C, Sun X, Zhang K, Anderson RE, 2009. DHA does not protect ELOVL4 transgenic mice from retinal degeneration. Mol. Vis 15, 1185–1193. [PubMed: 19536303]

Li S, Chen D, Sauve Y, McCandless J, Chen YJ, Chen CK, 2005. Rhodopsin-iCre transgenic mouse line for Cre-mediated rod-specific gene targeting. Genesis 41, 73–80. [PubMed: 15682388]

Li W, Chen Y, Cameron DJ, Wang C, Karan G, Yang Z, Zhao Y, Pearson E, Chen H, Deng C, Howes K, Zhang K, 2007a. Elovl4 haploinsufficiency does not induce early onset retinal degeneration in mice. Vis. Res 47, 714–722. [PubMed: 17254625]

Li W, Sandhoff R, Kono M, Zerfas P, Hoffmann V, Ding BC, Proia RL, Deng CX, 2007b. Depletion of ceramides with very long chain fatty acids causes defective skin permeability barrier function, and neonatal lethality in ELOVL4 deficient mice. Int. J. Biol. Sci 3, 120–128.

Liu A, Terry R, Lin Y, Nelson K, Bernstein PS, 2013. Comprehensive and sensitive quantification of long-chain and very long-chain polyunsaturated fatty acids in small samples of human and mouse retina. J. Chromatogr. A 1307, 191–200. [PubMed: 23938082]

Liu IS, Chen JD, Ploder L, Vidgen D, van der Kooy D, Kalnins VI, McInnes RR, 1994. Developmental expression of a novel murine homeobox gene (Chx10): evidence for roles in determination of the neuroretina and inner nuclear layer. Neuron 13, 377–393. [PubMed: 7914735]

Liu X, Garriga P, Khorana HG, 1996. Structure and function in rhodopsin: correct folding and misfolding in two point mutants in the intradiscal domain of rhodopsin identified in retinitis pigmentosa. Proc. Natl. Acad. Sci. U.S.A 93, 4554–4559. [PubMed: 8643442]

Logan S, Agbaga MP, Chan MD, Brush RS, Anderson RE, 2014. Endoplasmic reticulum microenvironment and conserved histidines govern ELOVL4 fatty acid elongase activity. J. Lipid Res 55, 698–708. [PubMed: 24569140]

Logan S, Agbaga MP, Chan MD, Kabir N, Mandal NA, Brush RS, Anderson RE, 2013. Deciphering mutant ELOVL4 activity in autosomal-dominant Stargardt macular dystrophy. Proc. Natl. Acad. Sci. U.S.A 110, 5446–5451. [PubMed: 23509295]

Lukiw WJ, Cui JG, Marcheselli VL, Bodker M, Botkjaer A, Gotlinger K, Serhan CN, Bazan NG, 2005. A role for docosahexaenoic acid-derived neuroprotectin D1 in neural cell survival and Alzheimer disease. J. Clin. Invest 115, 2774–2783. [PubMed: 16151530]

Mandal MN, Ambasudhan R, Wong PW, Gage PJ, Sieving PA, Ayyagari R, 2004. Characterization of mouse orthologue of ELOVL4: genomic organization and spatial and temporal expression. Genomics 83, 626–635. [PubMed: 15028285]

Mandal NA, Tran JT, Zheng L, Wilkerson JL, Brush RS, McRae J, Agbaga MP, Zhang K, Petrukhin K, Ayyagari R, Anderson RE, 2014. In vivo effect of mutant ELOVL4 on the expression and function of wild-type ELOVL4. Investig. Ophthalmol. Vis. Sci 55, 2705–2713. [PubMed: 24644051]

Martin RE, Elliott MH, Brush RS, Anderson RE, 2005. Detailed characterization of the lipid composition of detergent-resistant membranes from photoreceptor rod outer segment membranes. Invest. Ophthalmol. Vis. Sci 46, 1147–1154. [PubMed: 15790872]

Maugeri A, Meire F, Hoyng CB, Vink C, Van Regemorter N, Karan G, Yang Z, Cremers FP, Zhang K, 2004. A novel mutation in the ELOVL4 gene causes autosomal dominant Stargardt-like macular dystrophy. Investig. Ophthalmol. Vis. Sci 45, 4263–4267. [PubMed: 15557430]

McMahon A, Butovich IA, Kedzierski W, 2011. Epidermal expression of an Elovl4 transgene rescues neonatal lethality of homozygous Stargardt disease-3 mice. J. Lipid Res 52, 1128–1138. [PubMed: 21429867]

McMahon A, Butovich IA, Mata NL, Klein M, Ritter R 3rd, Richardson J, Birch DG, Edwards AO, Kedzierski W, 2007a. Retinal pathology and skin barrier defect in mice carrying a Stargardt disease-3 mutation in elongase of very long chain fatty acids-4. Mol. Vis 13, 258–272. [PubMed: 17356513]

McMahon A, Jackson SN, Woods AS, Kedzierski W, 2007b. A Stargardt disease-3 mutation in the mouse Elovl4 gene causes retinal deficiency of C32-C36 acyl phosphatidylcholines. FEBS Lett 581, 5459–5463. [PubMed: 17983602]

McMahon A, Lu H, Butovich IA, 2014. A role for ELOVL4 in the mouse meibomian gland and sebocyte cell Biology. Invest. Ophthalmol. Vis. Sci 55, 2832–2840. [PubMed: 24677106]

Mir H, Raza SI, Touseef M, Memon MM, Khan MN, Jaffar S, Ahmad W, 2014. A novel recessive mutation in the gene ELOVL4 causes a neuro-ichthyotic disorder with variable expressivity. BMC Med. Genet 15, 25. [PubMed: 24571530]

Mukherjee PK, Marcheselli VL, Serhan CN, Bazan NG, 2004. Neuroprotectin D1: a docosahexaenoic acid-derived docosatriene protects human retinal pigment epithelial cells from oxidative stress. Proc. Natl. Acad. Sci. U.S.A 101, 8491–8496. [PubMed: 15152078]

Musto AE, Gjorstrup P, Bazan NG, 2011. The omega-3 fatty acid-derived neuroprotectin D1 limits hippocampal hyperexcitability and seizure susceptibility in kindling epileptogenesis. Epilepsia 52, 1601–1608. [PubMed: 21569016]

Navidhamidi M, Ghasemi M, Mehranfard N, 2017. Epilepsy-associated alterations in hippocampal excitability. Rev. Neurosci 38 (3), 307–334.

Ohno Y, 2017. Elucidation of the synthetic mechanism of acylceramide, an essential lipid for skin barrier function. Yakugaku Zasshi 137, 1201–1208. [PubMed: 28966260]

Okuda A, Naganuma T, Ohno Y, Abe K, Yamagata M, Igarashi Y, Kihara A, 2010. Hetero-oligomeric interactions of an ELOVL4 mutant protein: implications in the molecular mechanism of Stargardt-3 macular dystrophy. Mol. Vis 16, 2438–2445. [PubMed: 21139992]

Olsson JE, Gordon JW, Pawlyk BS, Roof D, Hayes A, Molday RS, Mukai S, Cowley GS, Berson EL, Dryja TP, 1992. Transgenic mice with a rhodopsin mutation (Pro23His): a mouse model of autosomal dominant retinitis pigmentosa. Neuron 9, 815–830. [PubMed: 1418997]

Omura N, Li CP, Li A, Hong SM, Walter K, Jimeno A, Hidalgo M, Goggins M, 2008. Genome-wide profiling of methylated promoters in pancreatic adenocarcinoma. Cancer Biol. Ther 7, 1146–1156. [PubMed: 18535405]

Ozaki K, Doi H, Mitsui J, Sato N, Iikuni Y, Majima T, Yamane K, Irioka T, Ishiura H, Doi K, Morishita S, Higashi M, Sekiguchi T, Koyama K, Ueda N, Miura Y, Miyatake S, Matsumoto N, Yokota T, Tanaka F, Tsuji S, Mizusawa H, Ishikawa K, 2015. A novel mutation in ELOVL4 leading to spinocerebellar ataxia (SCA) with the hot cross bun sign but lacking erythrokeratodermia: a broadened spectrum of SCA34. JAMA Neurol 72, 797–805. [PubMed: 26010696]

Park YH, Jang WH, Seo JA, Park M, Lee TR, Park YH, Kim DK, Lim KM, 2012. Decrease of ceramides with very long-chain fatty acids and downregulation of elongases in a murine atopic dermatitis model. J. Invest. Dermatol 132, 476–479. [PubMed: 22158556]

Poirazi P, Brannon T, Mel BW, 2003a. Arithmetic of subthreshold synaptic summation in a model CA1 pyramidal cell. Neuron 37, 977–987. [PubMed: 12670426]

Poirazi P, Brannon T, Mel BW, 2003b. Pyramidal neuron as two-layer neural network. Neuron 37, 989–999. [PubMed: 12670427]

Poulos A, Johnson DW, Beckman K, White IG, Easton C, 1987. Occurrence of unusual molecular species of sphingomyelin containing 28–34-carbon polyenoic fatty acids in ram spermatozoa. Biochem. J 248, 961–964. [PubMed: 3435495]

Raz-Prag D, Ayyagari R, Fariss RN, Mandal MN, Vasireddy V, Majchrzak S, Webber AL, Bush RA, Salem N Jr., Petrukhin K, Sieving PA, 2006. Haploinsufficiency is not the key mechanism of pathogenesis in a heterozygous Elovl4 knockout mouse model of STGD3 disease. Investig. Ophthalmol. Vis. Sci 47, 3603–3611. [PubMed: 16877435]

Rohrbough J, Rushton E, Palanker L, Woodruff E, Matthies HJ, Acharya U, Acharya JK, Broadie K, 2004. Ceramidase regulates synaptic vesicle exocytosis and trafficking. J. Neurosci. : Off. J. Soc. Neurosci 24, 7789–7803.

Rowan S, Cepko CL, 2004. Genetic analysis of the homeodomain transcription factor Chx10 in the retina using a novel multifunctional BAC transgenic mouse reporter. Dev. Biol 271, 388–402. [PubMed: 15223342]

Sassa T, Kihara A, 2014. Metabolism of very long-chain Fatty acids: genes and pathophysiology. Biomol. Ther. (Seoul) 22, 83–92. [PubMed: 24753812]

Sherry DM, Hopiavuori BR, Stiles MA, Rahman NS, Ozan KG, Deak F, Agbaga MP, Anderson RE, 2017. Distribution of ELOVL4 in the developing and adult mouse brain. Front. Neuroanat 11.

Sommer JR, Estrada JL, Collins EB, Bedell M, Alexander CA, Yang Z, Hughes G, Mir B, Gilger BC, Grob S, Wei X, Piedrahita JA, Shaw PX, Petters RM, Zhang K, 2011. Production of ELOVL4

transgenic pigs: a large animal model for Stargardt-like macular degeneration. Br. J. Ophthalmol 95, 1749–1754. [PubMed: 21873315]

Soussi R, Boulland JL, Bassot E, Bras H, Coulon P, Chaudhry FA, Storm-Mathisen J, Ferhat L, Esclapez M, 2015. Reorganization of supramammillary-hippocampal pathways in the rat pilocarpine model of temporal lobe epilepsy: evidence for axon terminal sprouting. Brain Struct. Funct 220, 2449–2468. [PubMed: 24889162]

Stillwell W, Shaikh SR, Zerouga M, Siddiqui R, Wassall SR, 2005. Docosahexaenoic acid affects cell signaling by altering lipid rafts. Reprod. Nutr. Dev 45, 559–579. [PubMed: 16188208]

Stillwell W, Wassall SR, 2003. Docosahexaenoic acid: membrane properties of a unique fatty acid. Chem. Phys. Lipids 126, 1–27. [PubMed: 14580707]

Sudhof TC, Rizo J, 2011. Synaptic vesicle exocytosis. Cold Spring Harbor perspectives in biology 3.

Südhof TC, Rothman JE, 2009. Membrane fusion: grappling with SNARE and SM proteins. Science 323, 474–477. [PubMed: 19164740]

Tran HV, Moret E, Vaclavik V, Marcelli F, Abitbol MM, Munier FL, Schorderet DF, 2016. Swiss family with dominant stargardt disease caused by a recurrent mutation in the ELOVL4 gene. Klin Monbl Augenheilkd 233, 475–477. [PubMed: 27116512]

Uchida Y, Holleran WM, 2008. Omega-O-acylceramide, a lipid essential for mammalian survival. J. Dermatol. Sci 51, 77–87. [PubMed: 18329855]

Vasireddy V, Jablonski MM, Khan NW, Wang XF, Sahu P, Sparrow JR, Ayyagari R, 2009. Elovl4 5-bp deletion knock-in mouse model for Stargardt-like macular degeneration demonstrates accumulation of ELOVL4 and lipofuscin. Exp. Eye Res 89, 905–912. [PubMed: 19682985]

Vasireddy V, Jablonski MM, Mandal MN, Raz-Prag D, Wang XF, Nizol L, Iannaccone A, Musch DC, Bush RA, Salem N Jr., Sieving PA, Ayyagari R, 2006. Elovl4 5-bp-deletion knock-in mice develop progressive photoreceptor degeneration. Investig. Ophthalmol. Vis. Sci 47, 4558–4568. [PubMed: 17003453]

Vasireddy V, Uchida Y, Salem N Jr., Kim SY, Mandal MN, Reddy GB, Bodepudi R, Alderson NL, Brown JC, Hama H, Dlugosz A, Elias PM, Holleran WM, Ayyagari R, 2007. Loss of functional ELOVL4 depletes very long-chain fatty acids (> or =C28) and the unique omega-O-acylceramides in skin leading to neonatal death. Hum. Mol. Genet 16, 471–482. [PubMed: 17208947]

Vasireddy V, Vijayasarathy C, Huang J, Wang XF, Jablonski MM, Petty HR, Sieving PA, Ayyagari R, 2005. Stargardt-like macular dystrophy protein ELOVL4 exerts a dominant negative effect by recruiting wild-type protein into aggresomes. Mol. Vis 11, 665–676. [PubMed: 16163264]

Wachtmeister L, 1998. Oscillatory potentials in the retina: what do they reveal. Prog. Retin. Eye Res 17, 485–521. [PubMed: 9777648]

Wassall SR, Stillwell W, 2008. Docosahexaenoic acid domains: the ultimate non-raft membrane domain. Chem. Phys. Lipids 153, 57–63. [PubMed: 18343224]

Weidinger S, Novak N, 2016. Atopic dermatitis. Lancet 387, 1109–1122. [PubMed: 26377142]

Wen XH, Shen L, Brush RS, Michaud N, Al-Ubaidi MR, Gurevich VV, Hamm HE, Lem J, Dibenedetto E, Anderson RE, Makino CL, 2009. Overexpression of rhodopsin alters the structure and photoresponse of rod photoreceptors. Biophys. J 96, 939–950. [PubMed: 19186132]

Wheeler TG, Benolken RM, Anderson RE, 1975. Visual membranes: specificity of fatty acid precursors for the electrical response to illumination. Science 188, 1312–1314. [PubMed: 1145197]

Yu M, Benham A, Logan S, Brush RS, Mandal MN, Anderson RE, Agbaga MP, 2012. ELOVL4 protein preferentially elongates 20:5n3 to very long chain PUFAs over 20:4n6 and 22:6n3. J. Lipid Res 53, 494–504. [PubMed: 22158834]

Zadravec D, Tvrdik P, Guillou H, Haslam R, Kobayashi T, Napier JA, Capecchi MR, Jacobsson A, 2011. ELOVL2 controls the level of n-6 28:5 and 30:5 fatty acids in testis, a prerequisite for male fertility and sperm maturation in mice. J. Lipid Res 52, 245–255. [PubMed: 21106902]

Zerbinati C, Caponecchia L, Rago R, Leoncini E, Bottaccioli AG, Ciacciarelli M, Pacelli A, Salacone P, Sebastianelli A, Pastore A, Palleschi G, Boccia S, Carbone A, Iuliano L, 2016. Fatty acids profiling reveals potential candidate markers of semen quality. Andrology 4, 1094–1101. [PubMed: 27673576]

Zhang K, Kniazeva M, Han M, Li W, Yu Z, Yang Z, Li Y, Metzker ML, Allikmets R, Zack DJ, Kakuk LE, Lagali PS, Wong PW, MacDonald IM, Sieving PA, Figueroa DJ, Austin CP, Gould RJ, Ayyagari R, Petrukhin K, 2001. A 5-bp deletion in ELOVL4 is associated with two related forms of autosomal dominant macular dystrophy. Nat. Genet 27, 89–93. [PubMed: 11138005]

Zhang XM, Yang Z, Karan G, Hashimoto T, Baehr W, Yang XJ, Zhang K, 2003. Elovl4 mRNA distribution in the developing mouse retina and phylogenetic conservation of Elovl4 genes. Mol. Vis 9, 301–307. [PubMed: 12847421]

Zhou Q, Lai Y, Bacaj T, Zhao M, Lyubimov AY, Uervirojnangkoorn M, Zeldin OB, Brewster AS, Sauter NK, Cohen AE, Soltis SM, Alonso-Mori R, Chollet M, Lemke HT, Pfuetzner RA, Choi UB, Weis WI, Diao J, Sudhof TC, Brunger AT, 2015. Architecture of the synaptotagmin-SNARE machinery for neuronal exocytosis. Nature 525, 62–67. [PubMed: 26280336]
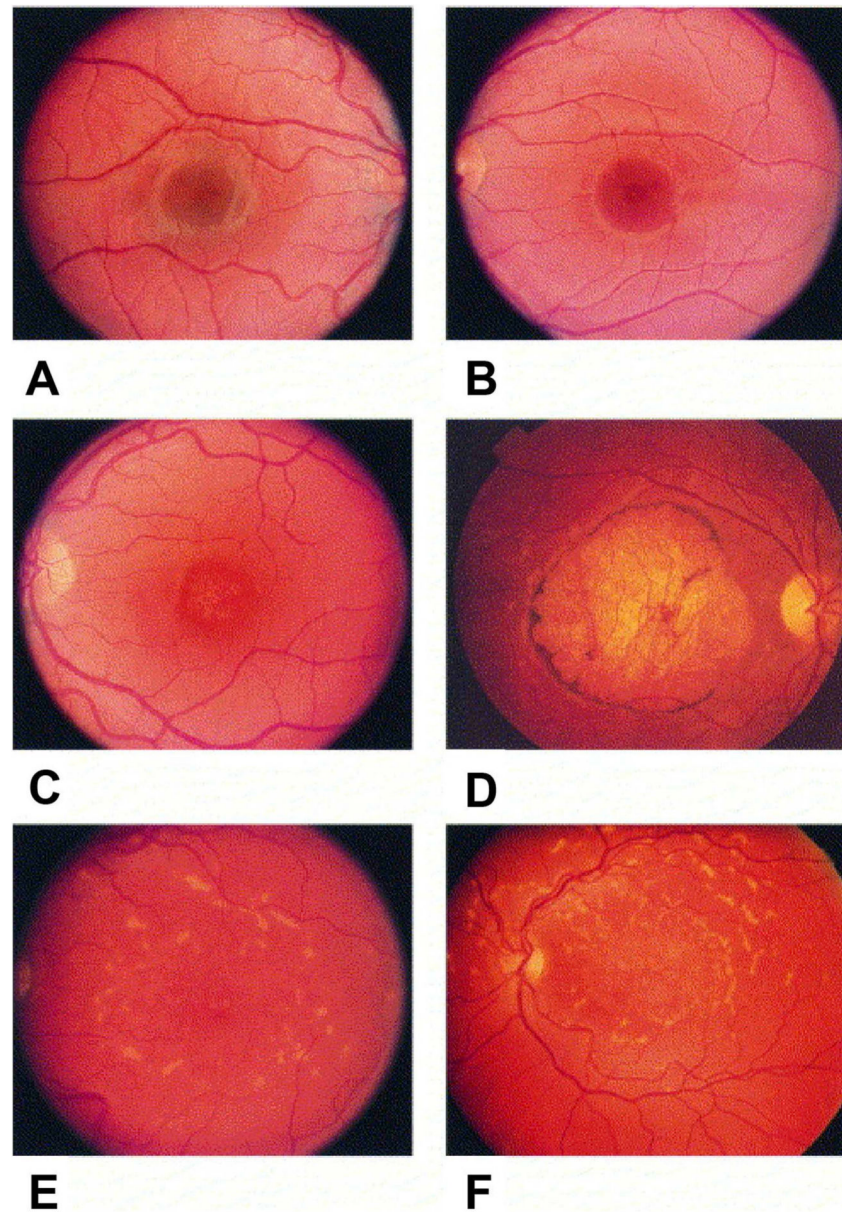
Fig. 1.
Fundus photographs of family members inheriting the autosomal dominant Stargardt-like macular dystrophy gene that illustrate the typical phenotype and longitudinal follow-up. (**A**) Right eye of a 5-year-old boy (B VI-9) with disease haplotype and normal fundus. (**B**) Left eye of a 9-year-old boy (B VI-6) with visual acuity of 20/20, 1-year course of hemeralopia, and early foveal atrophy. (**C**) Left eye of a 29-year-old man (B V-23) with typical early lesion without flecks. (**D**) Right eye of a 58-year-old man (A IV-25) with typical late lesion with flecks. (**E** and **F**) Longitudinal follow-up of left-eye of woman (B III-15) at ages 45 (**E**) and 53 (**F**); note the increasing macular atrophy and fundus flecks. **Reproduced with permissions from:** *Edwards* et al. *(1999). American Journal of Ophthalmology, Vol. 127, Issue 4, Page: 426–435, ISSN 0002-9394.* doi.org/10.1016/S0002-9394(98)00331-6. © 1999 Elsevier Science Inc.
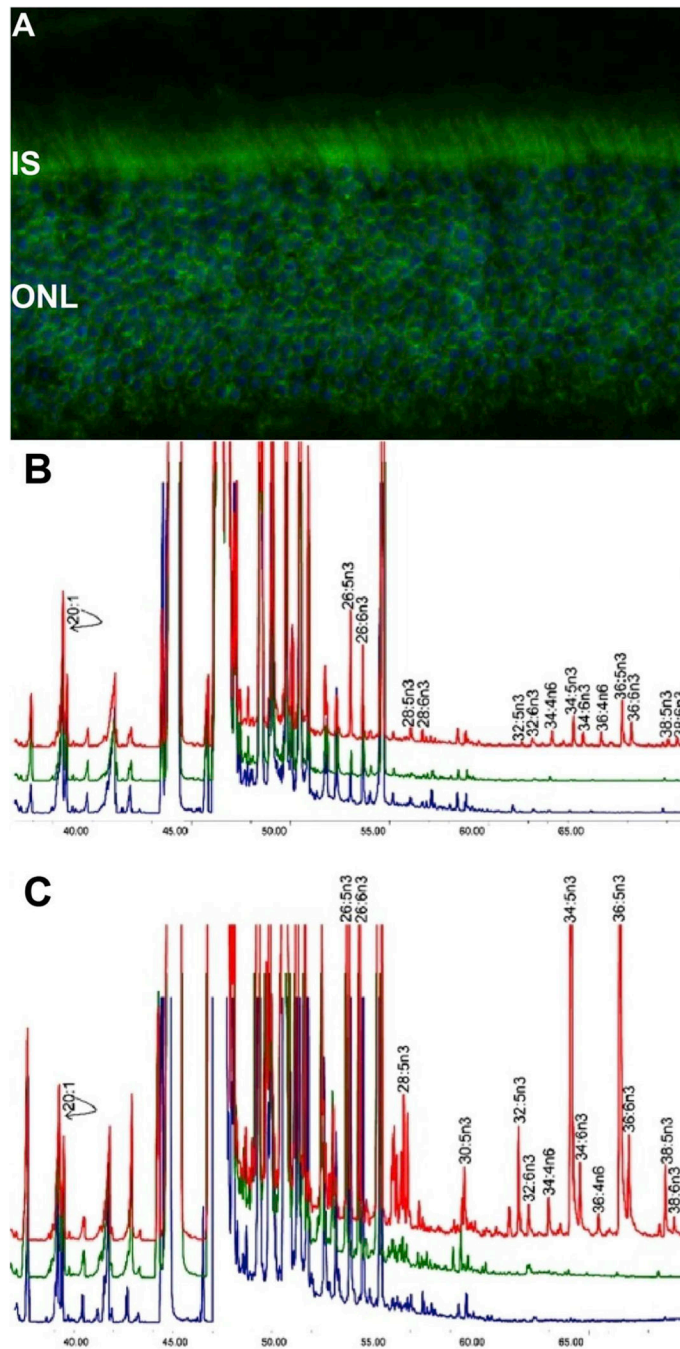
Fig. 2.
(**A**) ELOVL4 immunolabeling is detected in mouse retina, using affinity-purified ELOVL4 antibodies (green). Nuclei were stained with 4′,6-diamidino-2-phenylindole (blue). Images were captured by using an Olympus FluoView Confocal Microscope with 60X objective lens. IS, inner segments of rod and cone photoreceptors; ONL, outer nuclear layer. (**B**) Rat cardiomyocytes expressing ELOVL4 (red) or GFP (green) and non-transduced cells (blue) were cultured without precursors for 72 h. All cells, irrespective of ELOVL4 expression, synthesized C22-C26 PUFA. ELOVL4 expression in the absence of precursors resulted

in elongation of endogenous precursor to C28-C38 VLC-PUFA. (**C**) Cardiomyocytes in B above, cultured with 20:5n3 synthesized C24-C26 in all treatment groups. Significant biosynthesis of C28-C38 n3 VLC-PUFA occurred in Elovl4-transduced cells (red), but not in GFP (green) and non-transduced cells (blue), with accumulation of 34:5n3 and 36:5n3. Note that each chromatogram was normalized to endogenous 20:1, which did not change among the sample groups. **B & C are adapted reproductions from:** Agbaga et al. (2008). *Proceedings of the National Academy of Sciences, 105 (35) 12843–12848; DOI:* 10.1073/ pnas.0802607105.© 2008 by The National Academy of Sciences of the USA.
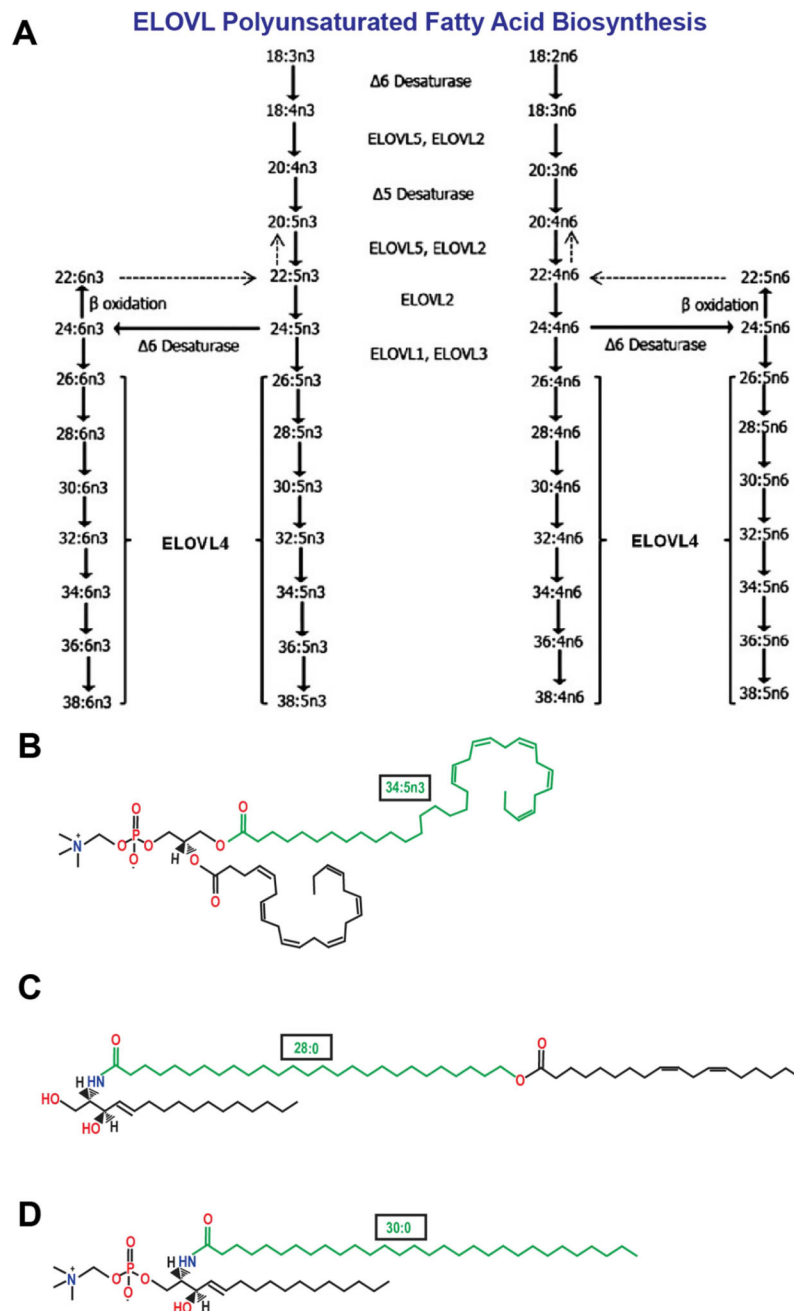
Fig. 3.

(**A**) Schematic *in vivo* biosynthetic pathway from 18:3n3 and 18:2n6 mediated by ELOVL4 and other ELOVL family proteins. Desaturase and elongation steps are consecutively performed by fatty acid desaturase-1 (FADS1 or 5 desaturase), fatty acid desaturase-2 (FADS2 or 6 desaturase), and ELOVL1–5. Although some elongases are specific for a single step, others are nonspecific or multi-functional and act at several steps (e.g., human ELOVL5 and murine ELOVL2). **A is an adapted reproduction from:** Man Yu et al. (2012). *J. Lipid Res. 53:(3) 494–504. doi:*10.1194/jlr.M021386. © 2012 by the American Society for Biochemistry and Molecular Biology, Inc. (**B**) Example of VLC-

PUFA esterification in the <u>retina</u>: phosphatidylcholine containing the VLC-PUFA, 34:5n3 and the LC-PUFA, 22:6n3 (DHA) (**C**) Example of VLC-SFA amidification in the <u>skin:</u> ω-O-acylceramide containing the VLC-SFA, 28:0 ω-O-linked with 18:2n3 (**D**) Example of VLC-SFA amidification in the <u>brain:</u> sphingomyelin containing the VLC-SFA, 30:0.
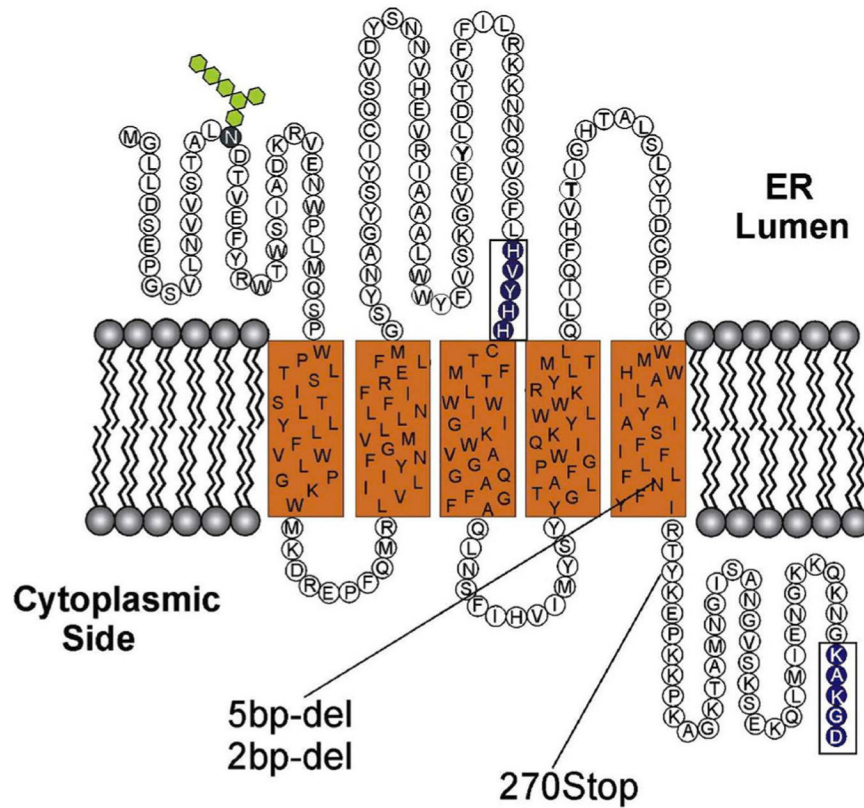
Fig. 4.
Predicted topological organization of ELOVL4 in the membrane based on SOUSI algorithm. The N-terminal segment contains an N-linked glycosylation site (hexagons) and therefore is on the lumen side of the ER membrane. In addition ELOVL4, like other members of the ELOVL family of elongases, contains a histamine cluster dideoxy binding motif [HVYHH] and a C-terminal dilysine ER retention motif [KAKGD]. The three Stargardt-like disease-associated mutations which result in a truncated protein lacking the C-terminus are also shown. **Reproduced with permissions from:** *Molday and Zhang (2010). Progress in lipid research, ISSN: 1873–2194, Vol: 49, Issue: 4, Page: 476–92.* doi.org/10.1016/j.plipres.2010.07.002. © 2010 Elsevier Ltd.
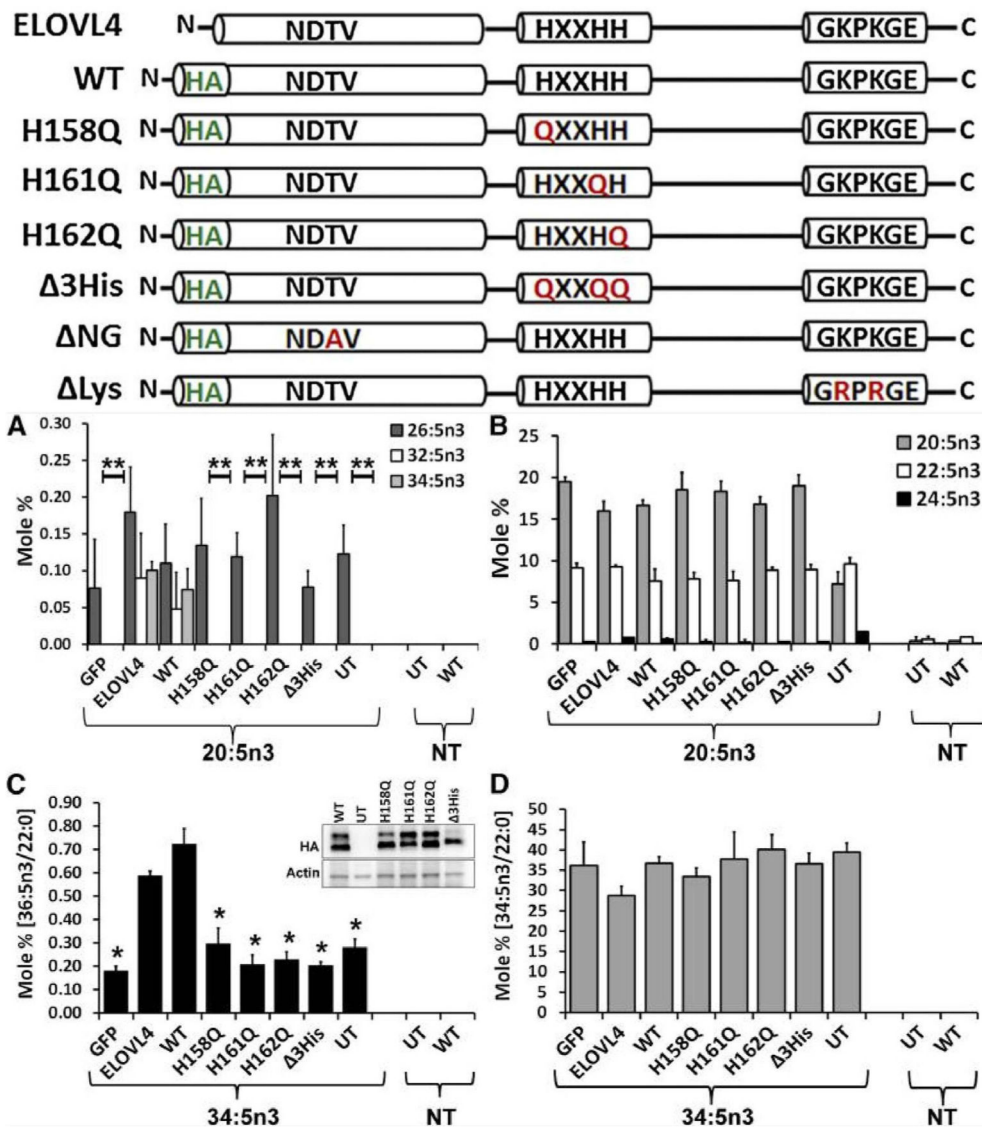
Fig. 5.

ELOVL4 active site mutants are deficient in VLC-PUFA biosynthesis. Schematic representation of untagged (ELOVL4) and HA-ELOVL4 constructs indicating individual mutations in active site (H158Q, H161Q, H162Q, and triple mutant Δ3His), N-glycosylation mutant (T22A; ΔNG), and lysine mutant (K308, 310R; ΔLys). (**A**) Elongation of 20:5n3 in HEK293T cells to 32:5n3 and 34:5n3 in ELOVL4 and WT, but not in catalytic dead mutants (histidine mutants) or GFP-expressing and UT controls. (**B**) Relative mole percent of 20:5n3, 22:5n3, and 24:5n3 with and without (NT) supplementation showing comparable levels of these FAs across samples in transduced HEK293T cells. (**C**) Elongation of 34:5n3 to 36:5n3 normalized to 22:0 in HEK293T cells expressing ELOVL4 and WT, but not in active site mutants, which were comparable to controls (GFP and UT). Data are represented as the mean ± SD (n = 3). Significance was assessed in comparison to WT; *P < 0.05; **P < 0.01. (Inset: adenoviral-mediated expression of HA-ELOVL4 proteins supplemented with either 20:5n3 or 34:5n3). (**D**) Levels of 34:5n3 internalized across treated and NT samples

showing comparable levels of the precursor. **Adapted reproduction with permissions from:** Logan et al. (2014). *J Lipid Res. Apr; 55(4): 698–708. doi:*10.1194/jlr.M045443. © 2014 by the American Society for Biochemistry and Molecular Biology, Inc. https://creativecommons.org/licenses/by/3.0/.
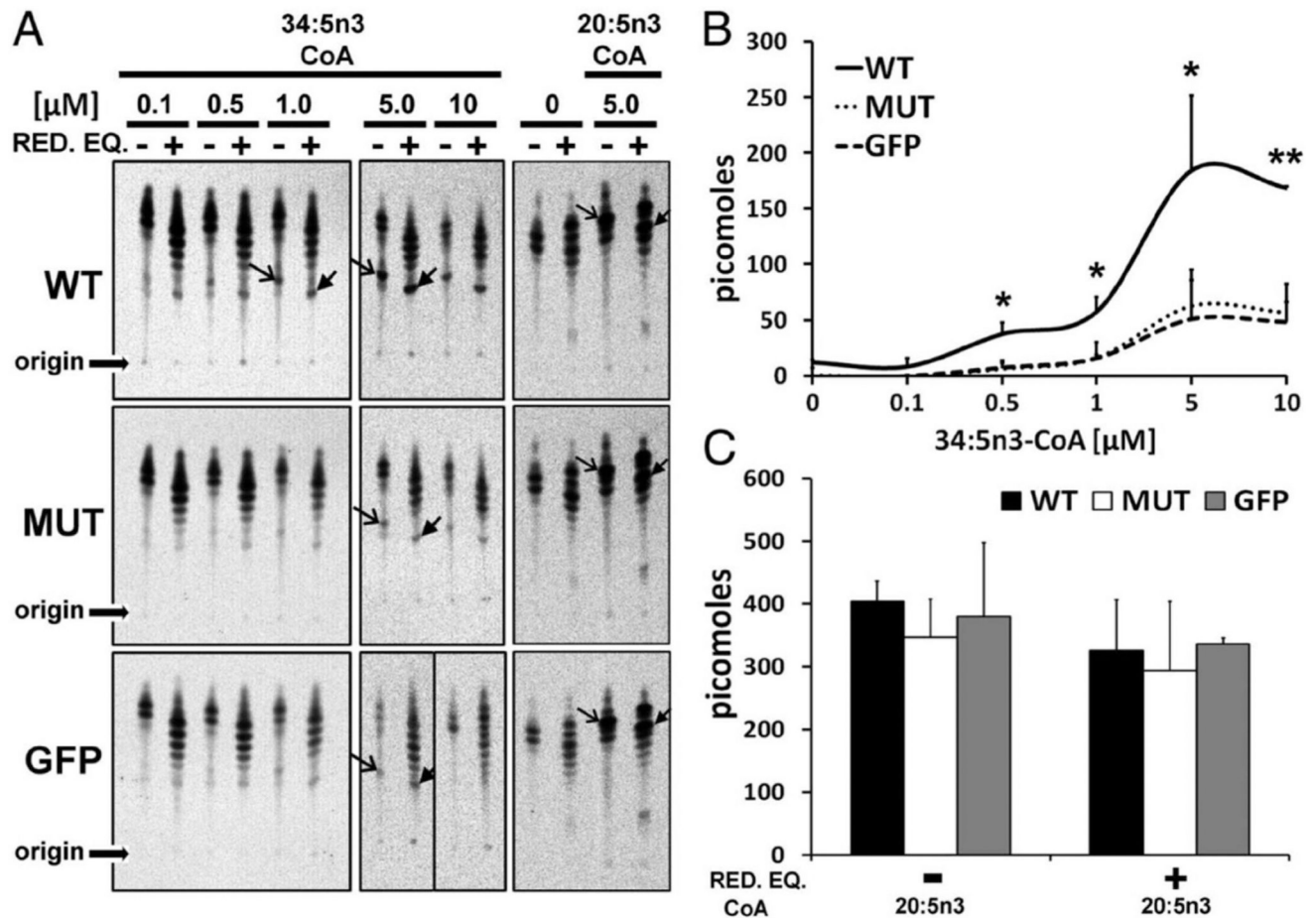
Fig. 6.

STGD3 mutant lacks innate condensation activity. (**A**) WT microsomes mediated the condensation of 34:5n3-CoA (open arrow heads), which was elongated in the presence (+) but not absence (−) of NADPH/NADH (RED.EQ; closed arrow heads), whereas MUT activity was comparable with GFP control. Condensation and elongation activity to 20:5n3-CoA and in the absence of exogenous substrate (lane "0") were comparable across samples. Origin of samples spotted on TLC is indicated. (**B**) WT generated more condensation product with increasing amounts of substrate (34:5n3-CoA) and a maximal specific activity of 200 pmol, whereas MUT was comparable with GFP control (*$P < 0.05$, **$P < 0.01$). (**C**) Quantitation of condensation and elongation activities to 20:5n3-CoA shows comparable activity across samples. **Reproduced with permissions from:** *Logan et al. (2013). PNAS. Apr. 2.110(14) 5446–5451;* https://doi.org/10.1073/pnas.1217251110 © 2013 Freely available online through the PNAS open access option. https://creativecommons.org/licenses/by-nc-nd/4.0/.
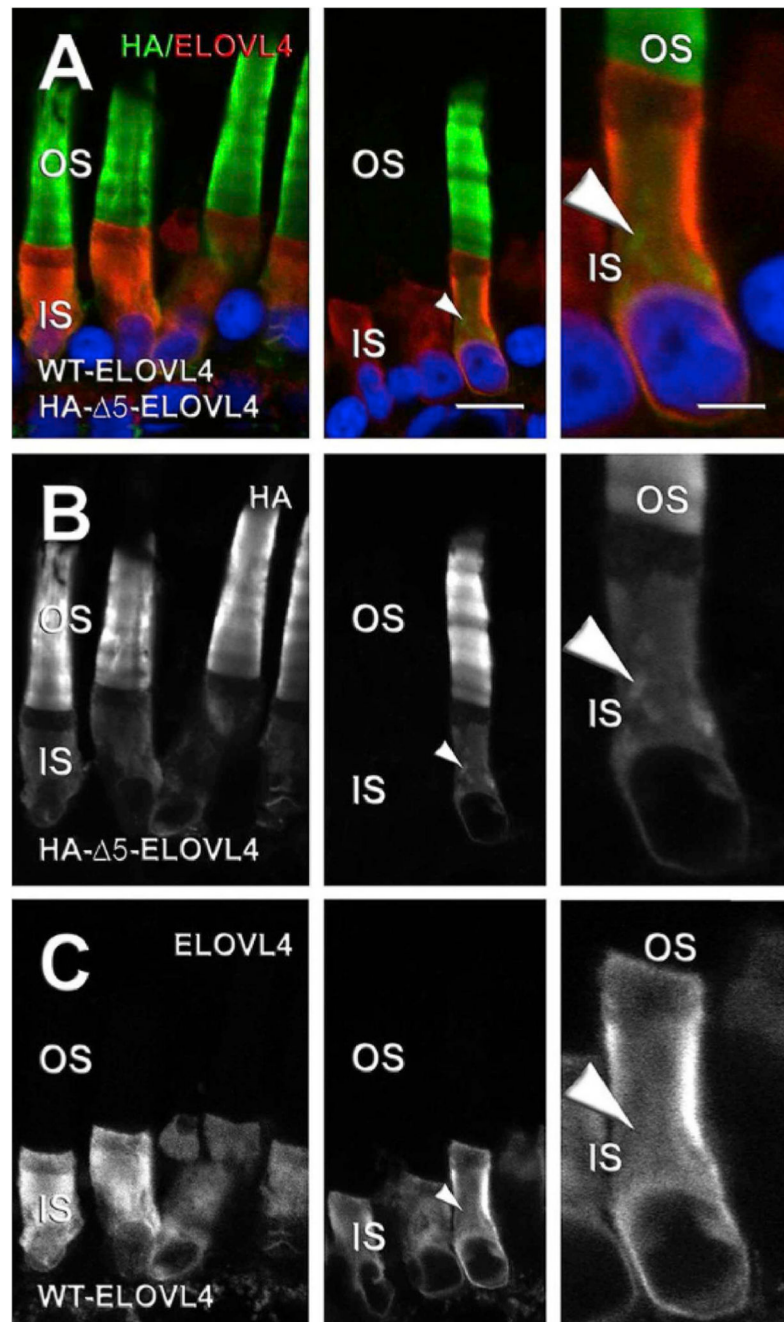
Fig. 7.
Effect of co-expression of HA- 5-ELOVL4 and WT ELOVL4 on mislocalization of WT
ELOVL4 to photoreceptor OS. (**A**–**C**) Confocal micrographs of *X. laevis* rod photoreceptor
cells co-expressing WT ELOVL4 (ELOVL4, red) and HA- 5-ELOVL4 (HA, green) with
Hoescht 33342 (blue) (n = 5). WT ELOVL4 expression was restricted to IS without any OS
localization (**A**, **C**), whereas HA- 5-ELOVL4 was distributed within IS and OS membranes
(**A**, **B**). White arrowheads indicate internal IS membranes (likely Golgi) that are HA-positive
and ELOVL4-negative. Left and center are from different transgenic retinas. Right shows
higher magnification. Scale bars: 4 and 10 μm. **Author reproduction from:** Agbaga et

al. (2014) *Investigative Ophthalmology & Visual Science June 2014, Vol.55, 3669–3680. doi:*10.1167/iovs.13-13099. © 2014 Association for Research in Vision and Ophthalmology.
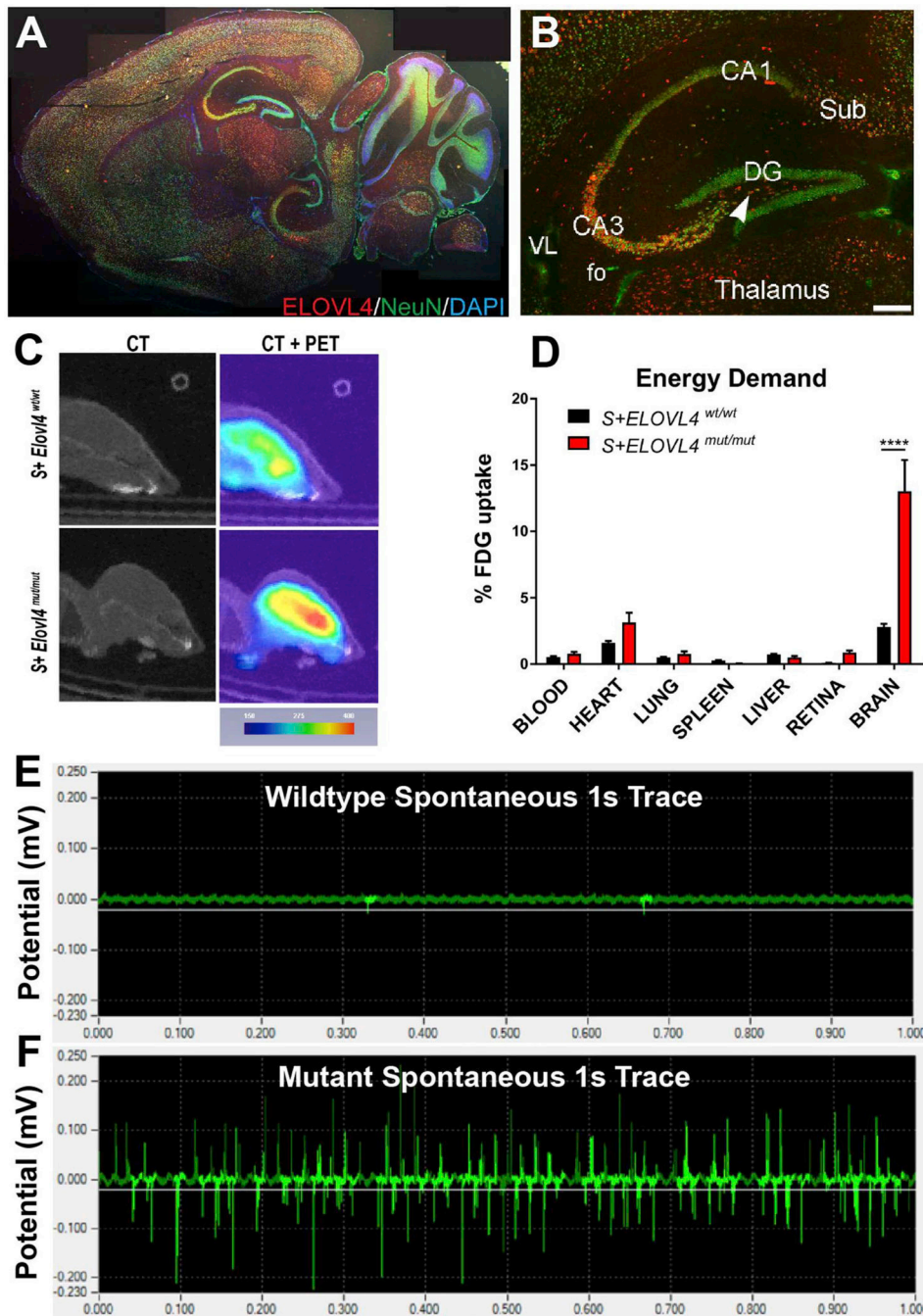
Fig. 8.
(**A**) ELOVL4 expression in *S+Elovl4^wt/wt^* mouse at P20. (**B**) Distribution of ELOVL4 (red) co-localized with the neuronal nuclear marker NeuN (green) in the hippocampal formation in *S^+Elovl4^wt/wt^* mouse at P20. Cornu Ammonis field 3 (CA3), polymorph layer (arrow), Cornu Ammonis field 1 (CA1), dentate gyrus (DG), subiculum (Sub), fo (fornix), VL (lateral ventricle). Scale bar = 250 μm. (**C**) Qualitative positron emission tomography (PET) imaging of *S^+ELOVL4^wt/wt^* and *S^+ELOVL4^mut/mut^* mice. (**D**) Post-mortem tissue quantification of FDG radioactivity in *S^+ELOVL4^wt/wt^* and *S^+ELOVL4^mut/mut^* mice.

Statistics: Multiple t-tests per row, Holm-Sidak's multiple comparisons correction, ****
= p < 0.0001. (**E**) This is an example of a 1s control tracing (*top*) qualitatively compared
to a 1s tracing from a spontaneous seizure event that was captured in 2 slices from an
$S^+Elovl4^{mut/mut}$ mouse (*bottom*). There is no stimulation here and although this was not
typical of *ex vivo* recordings for these mice, it emphasizes that the synaptic dysregulation in
these animals is capable of inducing itself into a seizure event of this magnitude in a slice
without any external stimulation. **Author adaptation from:** *Hopiavuori, B.R.* et al., *(2018).
Mol Neurobiol 55: 1795*. doi.org/10.1007/s12035-017-0824-8. © 2017 The Author(s).
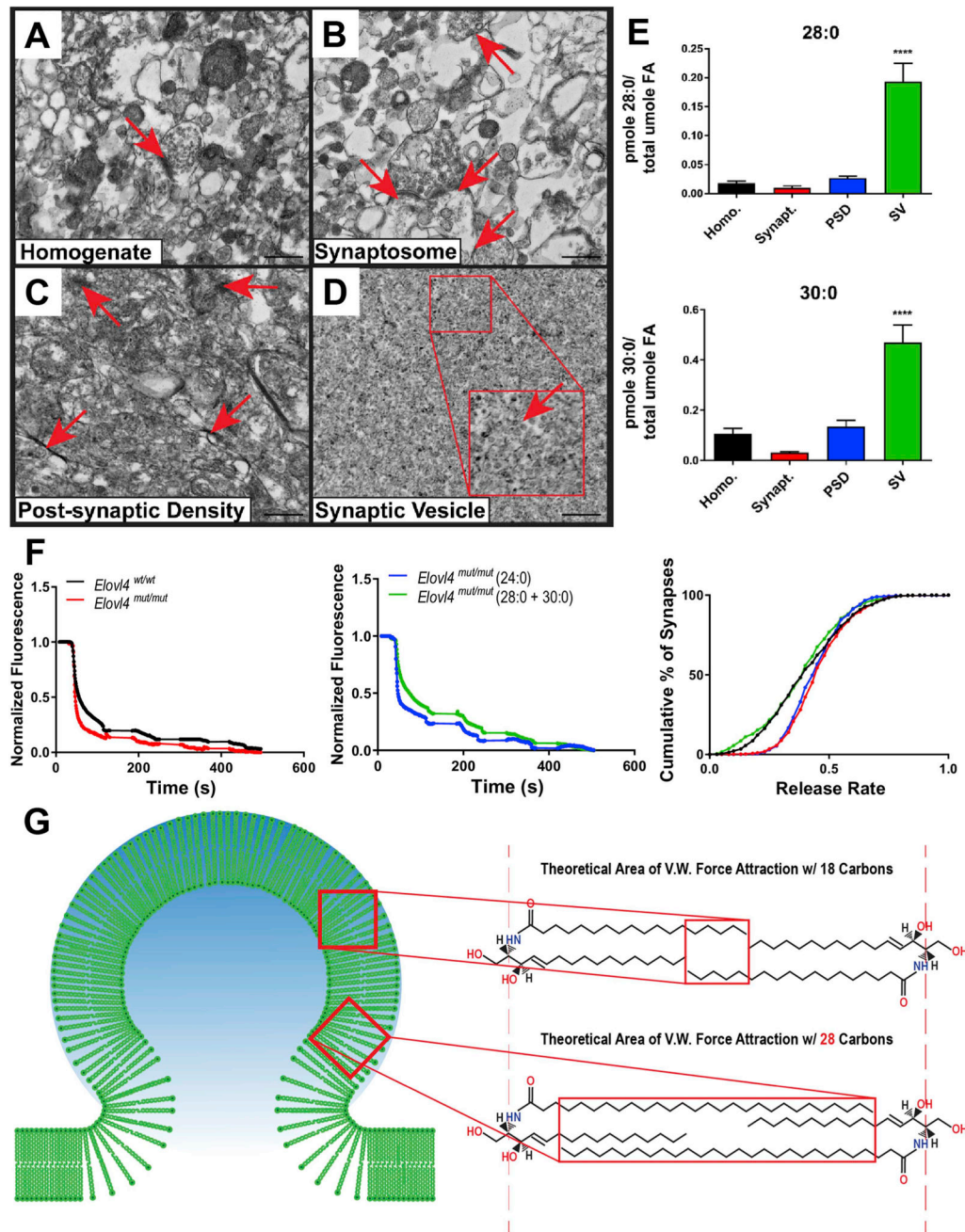
Fig. 9.
(**A**) Electron micrographs of synaptic fractions isolated from baboon hippocampus by sucrose gradient centrifugation (scale bar = 500 nm).Starting homogenate (Homo.) with a single neurosynaptosomal unit (arrow). (**B**) Neurosynaptosomal fraction (Synapt.) with multiple neurosynaptosomes in frame (arrows). (**C**) Post-synaptic density fraction (PSD) with multiple isolated densities indicated (arrows). (**D**) Synaptic vesicle fraction (SV) with high purity, vesicle indicated in zoomed inset (arrow). (**E**) Lipidomic analysis (GC-MS followed by GC-FID) reveals enrichment of both 28:0 and 30:0 in synaptic vesicle membranes relative to the other synaptic fractions. Statistics: 2-Way ANOVA with Tukey's

multiple comparison test, **** = p < 0.0001 (n = 3) error ± SEM. (**F**) Dysregulation of synaptic vesicle release in mutant neurons lacking ELOVL4. FM1–43 fluorometric assessment of synaptic vesicle release rates and pool size in E18.5 primary hippocampal cultures collected from *Elovl4$^{wt/wt}$* and *Elovl4$^{mut/mut}$* embryos ± treatment with either 28:0 + 30:0 that is missing in the mutant neurons, or 24:0, which is made by both mutant and wild-type neurons, as a control. [*Left*] Representative destaining curves comparing release rates in WT (black) and mutant animals (red) in response to high K$^+$ depolarization. [*Middle*] Representative destaining curves comparing release rates in mutant animals supplemented with either 24:0 (blue) or 28:0 + 30:0 (green) in response to high K$^+$ depolarization. [*Right*] Cumulative distribution of release rates for all synapses measured (Kolmogorov–Smirnov non-parametric examination of equality, p < 0.001). (**G**) One proposed theoretical model demonstrating a biophysical role for these very long-chain saturated products in supplying neurons with the means to down-regulate or resist its own calcium-mediated drive to release. Interaction between VLC-SFA by van der Waals (V.W.) forces could serve to stabilize vesicle membranes and impose a natural energy barrier that must be overcome in order to fine-tune the kinetics of pre-synaptic vesicle release in the brain. **Author adaptation from:** *Hopiavuori, B.R.* et al.*, (2018). Mol Neurobiol 55: 1795*. doi.org/10.1007/s12035-017-0824-8. © 2017 The Author(s).
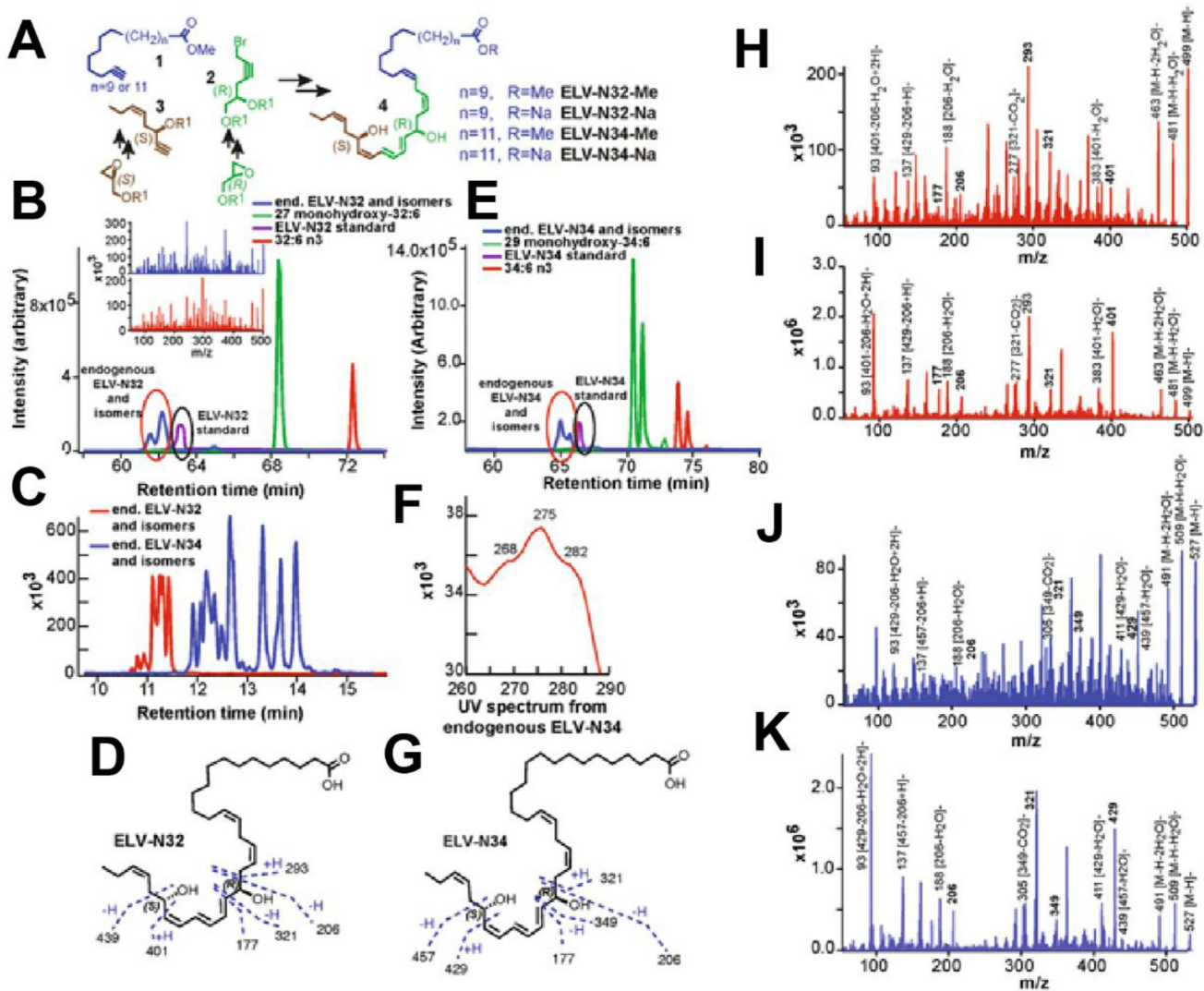
Fig. 10.

Discovery and structural characterization of ELV-N32 and ELV-N34 in primary human RPE cells in culture. (**A**) ELV-N32 and ELV-N34 were synthesized from three key intermediates (**1**, **2**, and **3**), each of which was prepared in stereochemically-pure form from readily-available starting materials. The stereochemistry of intermediates **2** and **3** was pre-defined by using enantiomerically-pure epoxide starting materials. The final ELVs (**4**) were assembled via iterative couplings of intermediates **1**, **2**, and **3**, and were isolated as methyl esters (Me) or sodium salts (Na). (**B**) 32:6n3 (red line), endogenous mono-hydroxy-32:6n3 (green line), and ELV-N32 (blue line) are shown with the ELV-N32 standard (purple). Multiple reaction monitoring of ELV-N32 shows two large peaks eluted earlier than the peak when standard ELV-N32 was eluted, displaying the same fragmentation patterns (shown in the insert spectra), suggesting that they are isomers. (**C**) Chromatogram for full daughter scans for ELV-N32 (red line) and ELV-N34 (blue line). (**D**) Fragmentation pattern of ELV-N32. (**E**) Same features as in (**B**) for 34:6n3 and ELV-N34. (**F**) UV spectrum of endogenous ELV-N34 showing triene features. (**G**) Fragmentation pattern of ELV-N32. (**H**) Full fragmentation

spectra of endogenous ELV-N32, and (**I**) the ELV-N32 standard shows that all major peaks from the standard match to the endogenous peaks. However, endogenous ELV-N32 has more fragments that do not show up in the standard, suggesting that it includes different isomers. (**J**) For ELV-N34, full fragmentation spectra of endogenous ELV-N34 peaks match up with the standard ELV-N34 (**K**), also suggesting the existence of ELV-N34 isomers. **Reproduced from:** *Bokkyoo Jun et al. (2017). Scientific Reports, Volume 7, Article number: 5279. doi:*10.1038/s41598-017-05433-7 © 2017 Creative Commons Attribution 4.0 International License: http://creativecommons.org/licenses/by/4.0/.

Table 1

Animal models of autosomal dominant Stargadt-like macular dystrophy (STGD3).

Model Details						Morphological Findings			
Name	Reported by	Species	Type	Mutation	Promoter	PR Degeneration	Retinal Organization	Ultrastructural Changes	Lipofuscin/A2E Accumulation
TG$^{l+,2+,3+}$	Karan (2005)	Mus musculus	transgenic	STGD3 (790–794 AACTT)	IRBP	rods and cones	ONL thinning	disorganized PR OS	yes
Elovl4$^{wt/-}$		Mus musculus	knockout	-	-	no	normal	-	-
Elovl4$^{wt/-}$	Raz-prag (2006)	Mus musculus	knockout	-	-	shortened ROS	normal	disorganized ROS discs	no
Elovl4$^{wt/mut}$	Vasireddy (2006)	Mus musculus	knock-in	Stgd3 (790–794 AACTT)	-	rods and cones	OPL Disorganization	shortened ROS	Lipofuscin
Elovl4$^{wt/stgd3}$	McMahon (2007)	Mus musculus	knock-in	Stgd3 (790–794 AACTT; c.813T > A; c.819A > T)	-	no	normal	no	Lipofuscin and A2E precursors
ELOVL4 (Tg. 5bp-del.)	Sommer (2011)	Sus scrofa domestica	transgenic	STGD3 (790–794 AACTT)	Rho4.4	rods and cones	ONL thinning and Disorganization	-	-
ELOVL4 (Y270terEYFP)	Sommer (2011)	Sus scrofa domestica	transgenic	STGD3 (p.Tyr270X)	Rho4.4	rods and cones	ONL thinning and Disorganization	-	-
Cone-cKO	Harkewicz (2012)	Mus musculus	conditional knockout		cre-HRGP	no	normal	no	Lipofuscin
Rod-cKO	Harkewicz (2012)	Mus musculus	conditional knockout		cre-Opsin	age-dependent loss of rods	normal	age-dependent loss of rods	Lipofuscin
Rod-cKO2	Barabas (2013)	Mus musculus	conditional knockout		Opsin-iCre75	no	normal	no	no
Chx10-cKO	Bennett (2014)	Mus musculus	conditional knockout		Chx10-cre	age-dependent loss of rods	ONL and OPL Disorganization	rod pre-synaptic vesicles reduced in size/number	no

Model Details						Functional Findings				
Name	Reported by	Species	Type	Mutation	Promoter	Scotopic a-wave	Scotopic b-wave	Photopic a-wave	Photopic b-wave	Occilatory Potential
TG$^{l+,2+,3+}$	Karan (2005)	Mus musculus	transgenic	STGD3 (790–794 AACTT)	IRBP	reduced	reduced	-	reduced	-
Elovl4$^{wt/-}$		Mus musculus	knockout	-	-	enhanced	normal	-	enhanced	-
Elavl4$^{wt/-}$	Raz-prag (2006)	Mus musculus	knockout	-	-	normal	normal	-	normal	-

Model Details						Functional Findings				
Name	Reported by	Species	Type	Mutation	Promoter	Scotopic a-wave	Scotopic b-wave	Photopic a-wave	Photopic b-wave	Occilatory Potential
Elovl4$^{wt/mut}$	Vasireddy (2006)	Mus musculus	knock-in	Stgd3 (790–794 AACTT)	-	enhanced	enhanced	enhanced	enhanced	-
Elovl4$^{wt/stgd3}$	McMahon (2007)	Mus musculus	knock-in	Stgd3 (790–794 AACTT; c.813T > A; c.819A > T)	-	reduced	reduced	-	normal	-
ELOVL4 (Tg. 5bp-del.)	Sommer (2011)	Sus scrofa domestica	transgenic	STGD3 (790–794 AACTT)	Rho4.4	-	reduced	-	reduced	-
ELOVL4 (Y270terEYFP)	Sommer (2011)	Sus scrofa domestica	transgenic	STGD3 (p.Tyr270X)	Rho4.4	-	reduced	-	reduced	-
Cone-cKO	Harkewicz (2012)	Mus musculus	conditional knockout	-	cre-HRGP	-	reduced	-	normal	-
Rod-cKO	Harkewicz (2012)	Mus musculus	conditional knockout	-	cre-Opsin	-	normal	-	reduced (flicker)	-
Rod-cKO2	Barabas (2013)	Mus musculus	conditional knockout	-	Opsin-iCre75	normal	normal	normal	normal	-
Chx10-cKO	Bennett (2014)	Mus musculus	conditional knockout	-	Chx10-cre	reduced	reduced	normal	normal	reduced

Table 2

Mutations in ELOVL4 that have been linked to human disease

Study First Reported	Mutation				Inheritance	Phenotype						
	Exon	Site	Mutation	Genetic Consequence		Macular Degeneration	Seizures	Spinocerebellar Ataxia	Ichthyosis	Erythrokeratodermia variabilis	Hypertonia	Leathality
Zhang et al. (2001)	6	c.797–801	del_AACTT	premature stop, truncation	Dominant	Y	N	N	N	N	N	N
Bernstein et al. (2001)	6	c.789, c.794	del_T, del_T	frameshift, truncation	Dominant	Y	N	N	N	N	N	N
Maugeri et al. (2004)	6	c.810	C > G	p.Tyr270X, truncation	Dominant	Y	N	N	N	N	N	N
Bardak et al. (2016)	6	c.814	G > C	p.E272Q, truncation	Dominant	Y	N	N	N	N	N	N
Bardak et al. (2016)	6	c.859	A > G	p.M299V, truncation	Dominant	Y	N	N	N	N	N	N
Aldahmesh et al. (2011)	5	c.646	C > T	p.Arg216X, truncation	Recessive	N	Y	N	Y	N	Y	Y
Aldahmesh et al. (2011)	6	c.690	del	p.Ile230Metfs*22, truncation	Recessive	N	Y	N	Y	N	Y	Y
Mir et al. (2014)	1	c.78	C > G	p.Tyr26*, truncation	Recessive	N	Y	N	Y	N	Y	Y
Cadieux-Dion et al. (2014)	4	c.540	G > C	p.L168F	Dominant	N	N	Y	N	Y	N	N
Bourassa et al. (2015)	6	c.736	T > G	p.W246G	Dominant	N	N	Y	N	N	N	N
Ozaki et al. (2015)	4	c.539	A > C	p.Gln80Pro	Dominant	N	N	Y	N	Y	N	N